USE OF REMOTE SENSING DATA IN A CROP GROWTH MODEL TO ESTIMATE ACTUAL CROP YIELDS

TESTING AQUACROP WITH NDVI TIME SERIES FOR TWO CROPS IN SPAIN

S. GANGARAM PANDAY

March, 2014

SUPERVISORS:
Dr. Ir. C.A.J.M. de Bie
Dr. Ir. A. Vrieling

USE OF REMOTE SENSING DATA IN A CROP GROWTH MODEL TO ESTIMATE ACTUAL CROP YIELDS

TESTING AQUACROP WITH NDVI TIME SERIES FOR TWO CROPS IN SPAIN

Thesis submitted to the Faculty of Geo-Information Science and Earth Observation of the University of Twente in partial fulfilment of the requirements for the degree of Master of Science in Geo-information Science and Earth Observation.
Specialization: Natural Resource Management

SUPERVISORS:
Dr. Ir. C.A.J.M. de Bie
Dr. Ir. A. Vrieling

THESIS ASSESSMENT BOARD:
Dr. Y.A. Hussin (Chair)
Prof. D. Raes (External Examiner, KU Leuven University)

ABSTRACT

Modelling and monitoring of crops is of importance to develop, implement and maintain food security policy. This is especially necessary in order to keep pace with the increasing needs of a growing world population. With the world's population estimated at 9.15 billion by 2050, food production will have to increase by 60% above current production levels. Fundamental to food security studies is to have accurate and timely knowledge of what is grown, where it is grown, and when and how much of it. Crop Growth Models (CGM) are increasingly being utilized for food production monitoring activities. They capture the relationship between the physiological processes within a plant, and its environment and by simulating these processes, crop growth and crop development is estimated and crop yield at harvest can be predicted.

The use of Remote Sensing data in FAO's crop growth model AquaCrop to estimate actual crop yields has been evaluated. Canopy cover and biomass, derived from coarse resolution NDVI time series, have been forced into AquaCrop for 641 barley and 695 durum wheat sample segments in Spain over five growing seasons between 2004 and 2009. It was found that forcing NDVI-derived canopy cover or biomass did not improve AquaCrop's performance, compared to the use of AquaCrop without forcing. The crop phenology in simulation runs (baseline, forced canopy cover, forced biomass) for the majority of selected samples does not agree with crop phenology derived from coarse resolution NDVI time series. Crop base temperature is suspect of being too low, however other crop parameters may be suspect as well. Calibration of the conservative crop parameters to achieve accurate and reliable estimations in AquaCrop is required.

Inaccuracies in biomass, canopy cover and CGP derived from the NDVI time series may also occur as a result of the coarse resolution in combination with segment heterogeneity. Sample segments are smaller than NDVI pixels while barley and durum wheat occupy only a small fraction in most sample segments. Utilization of higher spatial resolution NDVI time series, like MODIS or PROBA-V can be considered to address this. In addition the (complementary) use of SAR or inverse radiative transfer modelling may proof useful.

ACKNOWLEDGEMENTS

My sincere appreciation goes out to all, who have in more or less noticeable but ever essential ways supported me during this endeavour. I owe special thanks to my first supervisor, Dr. Kees de Bie, not only for awakening my interest in the subject, but also for his generously provided guidance. I also like to thank my second supervisor, Dr. Anton Vrieling, for his valuable pointers during the research and thesis writing. KU Leuven University's Professor Raes' cooperation and contribution have been fundamental to this research. My sincere gratitude goes out to him. A special appreciation is reserved for Willem Nieuwenhuis for his contribution and support in executing the model adjustments and simulations. Finally my deepest respect and appreciation is reserved for my family, for their love and support.

Why do we seek more knowledge
when we pay no heed
to what we know already?

(Sufi Wisdom-Shah Firoz †1660)

TABLE OF CONTENTS

LIST OF FIGURES

LIST OF TABLES

1. INTRODUCTION

1.1. Modelling and monitoring of crops

Modelling and monitoring of crops is of importance to develop, implement and maintain food security policy. This is especially necessary in order to keep pace with the increasing needs of a growing world population. The World Summit on How to Feed the World 2050 *High-level Expert Forum* (Rome 12-13 October 2009) already concluded that agriculture in the 21st century *"…has to produce more food and fibre to feed a growing population with a smaller rural labour force, more feed stocks for a potentially huge bioenergy market, contribute to overall development in the many agriculture-dependent developing countries, adopt more efficient and sustainable production methods and adapt to climate change"*. With the world's population estimated at 9.15 billion by 2050, food production will have to increase by 60% above current (2005/2007) production levels (Alexandratos & Bruinsma, 2012).

Fundamental to food security studies is to have accurate and timely knowledge of what is grown, where it is grown, and when and how much of it. Crop Growth Models (CGM) are increasingly being utilized for food production monitoring activities (Clevers et al., 2002). Crop growth models try to capture the relationship between the physiological processes within a plant, and its environment. By simulating these processes, usually in daily time steps, crop growth and crop development is estimated and crop yield at harvest can be estimated. Modelling of crop growth generally revolves around a crop growth engine. In essence, three main types of crop growth engines can be distinguished (Steduto, 2006) namely carbon-driven, solar-driven and water-driven crop growth engines. Figure 1.1 shows an overview of processes involved in vegetation biomass production, canopy transpiration and the different modelling pathways.

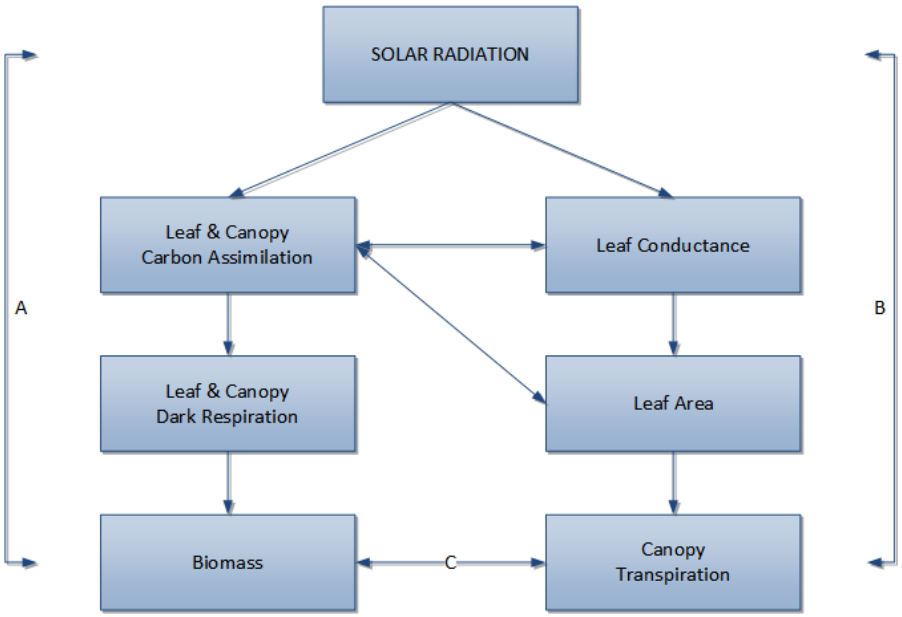

Figure 1.1. Overview of processes involved in vegetation biomass production, canopy transpiration and modelling pathways. Solar and carbon driven engines follow path A while water driven engines follow path C

(A= biomass production, B= canopy transpiration, C= linkage between biomass production and canopy transpiration)

(Adapted from Steduto, 2006)

Carbon-driven and solar-driven crop growth engines follow pathway A, while the water-driven crop engine follows pathway C. Table 1.1 below lists the advantages and disadvantages of the different engines and also provides examples of CGMs currently in use.

Table 1.1. Overview of advantages and disadvantages of different crop growth engines

	Carbon-driven	**Solar-driven**	**Water-driven**
Advantages	Hierarchical system organization Sound physical & physiological basis	Robust under non-stressed conditions Less complex	Robust Less complex
Disadvantages	Complex Cultivar specific Uncertainties (resulting in large errors in biomass estimations)	Inconsistent variability among crops, locations and years Nonlinear under stress conditions	Difficulties deriving actual crop transpiration
Crop Growth Models	Wageningen crop models (BACROS, SUCROS, ARID CROP, WOFOST, MACROS, PAPRAN, SWACROP etc.) American CROPGRO model series (SOYGRO, PNUTGRO, BEANGRO, TOMGRO etc.)	CERES EPIC STICS CropSyst	AquaCrop CropSyst

(Adapted from Steduto, 2006)

Different CGMs have been developed, used and tested over time for different crops and growth conditions. However crop yield estimation results have shown substantial variability in accuracy and robustness (Palosuo et al., 2011; Rötter et al., 2012). Many CGMs require an extensive amount of input data which hampers their applicability beyond research conditions. WOFOST for example (Vandiepen et al., 1989), which is used within the EU's Joint Research Centre's Monitoring Agricultural Resources Unit Mission (MARS), requires about 40 parameters to characterize the crop under evaluation (Khan, 2011; Todorovic et al., 2009). Recently the FAO has developed the AquaCrop CGM in an attempt to create optimal balance between simplicity, accuracy and robustness (Steduto et al., 2009). AquaCrop uses a relatively small number of parameters and input-variables and has been assessed for different crops in different circumstances with promising results (Abedinpour et al., 2012; Andarzian et al., 2011; Karunaratne et al., 2011; Khoshravesh et al., 2013; Mebane et al., 2013; Mkhabela & Bullock, 2012; Stricevic et al., 2011; Wellens et al., 2013).

The general absence of a spatial component in crop growth models is considered a serious shortcoming (Clevers et al., 2002) and this is especially so for yield estimations at regional scales. Determining model inputs for the required spatial and temporal dimensions is a burdensome task and assuming spatial homogeneity often leads to errors in estimated outputs (Launay & Guerif, 2005). There exists considerable uncertainty with regards to the spatial distribution of farm management practices and soil and weather conditions (Hansen & Jones, 2000). A hybrid approach, combining crop growth simulation modelling and remotely sensed data, has the potential to overcome both limitations of CGM's.

Remote sensing data can be used in CGM's in two ways. One is as input to CGM's, more specifically for meteorological variables (de Wit & van Diepen, 2008) at regional scale. Secondly, RS data can be integrated into CGM's, providing actual empirical information of the crop's growth state throughout the crop's lifecycle and can also in that way account for the spatial variability in the plants environment. The integration of RS data in CGMs can take different forms. Delécolle *et al.* (1992) distinguish two main approaches: forcing and recalibration. In forcing, model state variables are replaced or adjusted using remotely sensed estimations. In recalibration, model parameters or initial conditions are adjusted based on RS observations.

There is ample evidence showing that the integration of RS data in CGMs improves crop yield estimations. Many approaches utilize Leaf Area Index (LAI) derived from a vegetation index (Casa et al., 2012; Clevers et al., 2002; Doraiswamy et al., 2004; Ma et al., 2013; Myneni et al., 1995). Moriondo *et al.* (2007), not without success, utilize NDVI (Normalized Difference Vegetation Index) in combination with a CGM to estimate wheat yield on a regional scale in Italy. Alternatively also non-optical remote sensing data i.e. Advanced Synthetic Aperture Radar (ASAR) is utilized for LAI retrieval, sometimes in combination with optical remote sensing (Dente et al., 2008). In a recent study on wheat production in Andalusia, Spain (Khan, 2011), the use of RS data from thermal bands (Moderate Resolution Imaging Spectrometer Land Surface Temperature) for actual yield estimations showed very close agreement with measured yield data. Another study, on rice in the Mekong Delta in Vietnam, used a Soil-Leaf-Canopy (SLC) radiative transfer model for LAI estimation and forced this into an existing CGM (Ha, 2013), again showing close agreement with measured yield data.

Until now, RS data has mainly been integrated in complex CGMs, therefore still requiring extensive input datasets. With the recent developments regarding CGM's (FAO, 2012), effective incorporation of RS data in these models is a promising field of study that may improve the model's accuracy and applicability to larger regions (De Bie & Morsink, 2013). Figure 1.2 shows the evolution in crop yield assessment methods.

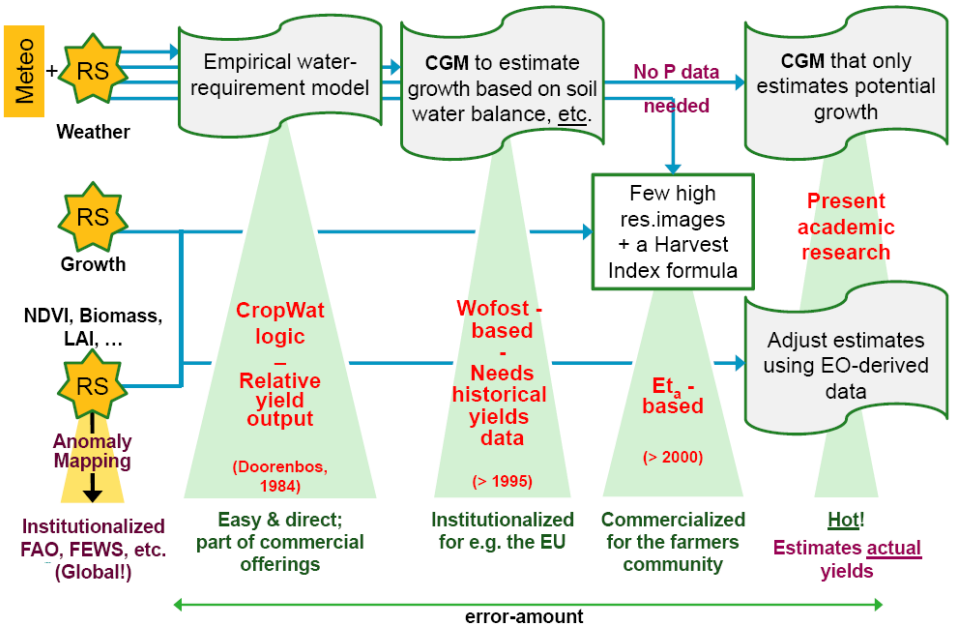

Figure 1.2. Evolution in crop yield assessment methods *(Source: de Bie & Morsink, 2013)*

In summary, accurate crop yield estimation with existing CGMs requires extensive input datasets and substantial efforts for calibration. Recent efforts have resulted in more simple and robust CGM's (i.e. FAO's AquaCrop), however the concerns with regards to input data requirements and calibration to achieve accurate and reliable estimations remain. RS data provides actual empirical data of the crop's growth state throughout the crop's lifecycle and its appropriate use in CGMs is likely to lead to more accurate and more robust actual yield estimation. This is especially important for yield estimations at the spatial scales necessary to support food security policy. Forcing with RS-data overrules the CGM's basic carbon, water or solar-driven engine, potentially reducing substantial ground-based data requirements, and uses the strengths of CGM's that defines partition and development, leading ultimately to yield.

1.2. AquaCrop, FAO's simulation model for crops

In an effort to integrate improved knowledge and understanding of soil-water-yield relationships into crop growth models (Steduto et al., 2009), the FAO has recently developed the AquaCrop CGM. At the basis of the model is the approach of Doorenbos and Kassam (1979) which relates the relative yield loss of a crop to the relative reduction in evapotranspiration. By separating crop transpiration and soil evaporation from evapotranspiration, the productive water use (i.e. crop transpiration) is utilized to establish yield estimations. Figure 1.3 provides a schematic overview of the AquaCrop model. For a more detailed explanation of AquaCrop, reference is made to FAO's Irrigation and Drainage paper 66, (FAO, 2012).

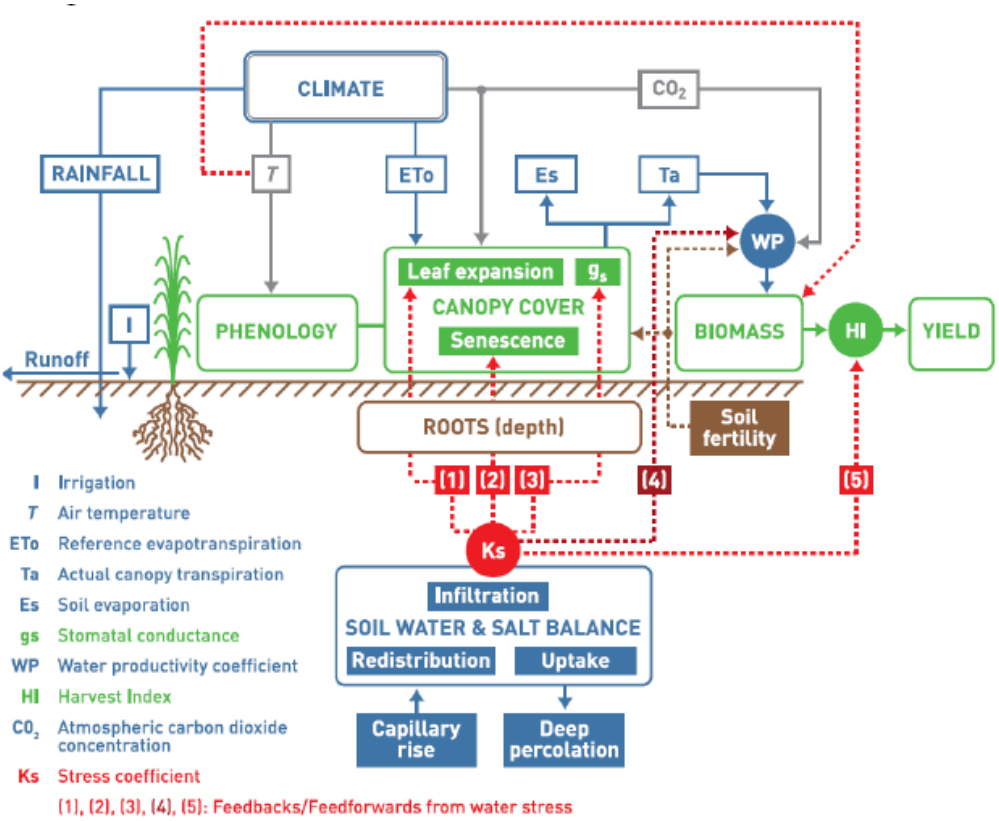

Figure 1.3. Schematic overview of AquaCrop *(Source: Steduto et al., 2008)*

AquaCrop uses weather, crop, soil and management data to estimate yield output. Table 1.2 summarizes AquaCrop's input data requirements. Weather parameters can be provided on a daily, 10-daily or monthly basis. CO_2 concentration data is provided for larger timescales (years, decades). Crop and soil data is provided once, while irrigation and management data is provided for each irrigation or management event.

Table 1.2. AquaCrop input data overview

Type of data	Description	Specific parameters
Weather	Characterizes the weather	Temperature Reference evapotranspiration Rainfall CO_2 concentration
Crop	Characterizes the crop	Crop temperature range Rooting depth Crop stage lengths Canopy growth & decline characteristics Soil water depletion factors
Soil	Characterizes the soil properties and profile	Number of soil horizons Thickness of soil horizons Water content at field capacity and Permanent wilting point Saturated hydraulic conductivity Restrictive layer depth
Irrigation	Specifies the irrigation	Irrigation method Date and depth for each irrigation event
Management	Specifies soil fertility and soil conservation practices that influence the soil-water balance	Soil fertility levels Reduction in runoff Mulching or soil bunds

AquaCrop calculates the simulated yield in a number of steps. Figure 1.4 shows AquaCrop's calculation scheme, including the feedback mechanisms which account for various stresses.

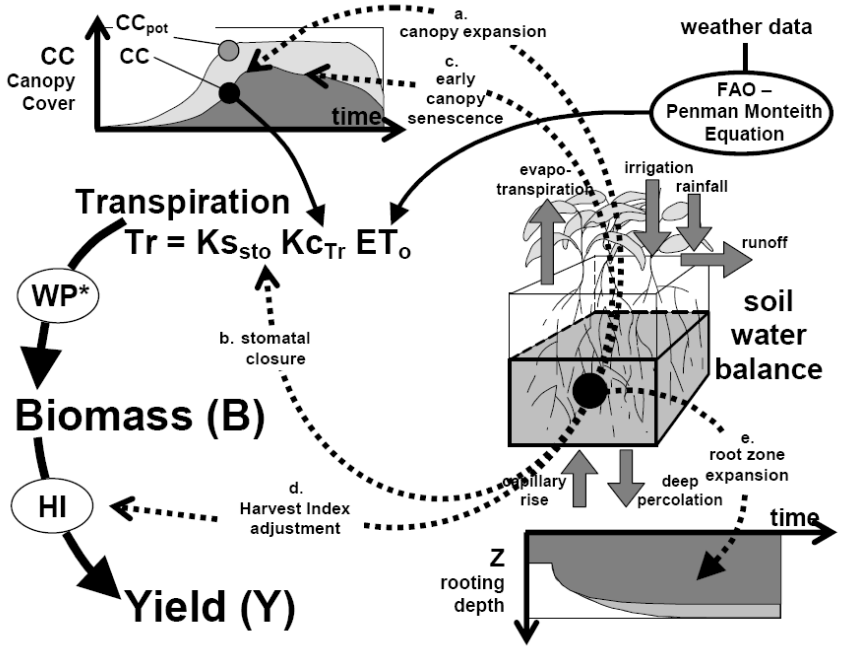

Figure 1.4. AquaCrop's calculation scheme (Source: Raes *et al.*, 2009)

Dotted arrows indicate processes affected by water stress. CC is the canopy cover, Ks the target process specific stress coefficient, WP is the water productivity, ET_o the reference evapotranspiration, HI the harvest index and Kc_{TR} the crop transpiration coefficient.

By simulating the soil water balance over time, considering crop, weather, soil, irrigation and management characteristics, the green canopy development, expressed as crop canopy cover, is estimated. From canopy cover, AquaCrop derives crop transpiration.

Biomass (aboveground) is subsequently derived from crop transpiration using the concept of normalized water productivity (Raes et al., 2009). In turn, the yield is derived from biomass using a harvest index. The simulations in AquaCrop are performed in daily time steps. For a detailed explanation of AquaCrop's calculation scheme, reference is made to FAO's Irrigation and Drainage paper 66, (FAO, 2012) and Raes *et al.* (2009)

1.3. Research objective

The research objective is to determine if the use of RS data through forcing within FAO's CGM AquaCrop, results in improved and accurate actual yield estimations. This will be tested using yield data of barley and durum wheat collected at the field level in Spain. For the purpose of this research, the use of RS data will be limited to directly estimating crop canopy cover and crop biomass from NDVI time series. A forcing data assimilation approach will be used, i.e. the model state variables for biomass and canopy cover will be adjusted or replaced daily by RS based estimations. Calibration of fixed model parameters and initial conditions is excluded in this study.

1.4. Research question and hypothesis

From the research objective, and assuming that RS data provide a good measure of biomass or canopy cover, the following research question has been derived:

- Does the use of biomass and/or canopy cover derived from RS data within AquaCrop, result in more accurate actual yield estimations compared to AquaCrop's yield estimations without the use of RS data?

The research question can be reformulated into the following hypothesis:

- H_0 : The accuracy of actual yield estimations in the AquaCrop model that utilizes RS data is less than or equal to the accuracy of yield estimations derived from the AquaCrop model without the use of RS data.
- H_A : The accuracy of actual yield estimations in the AquaCrop model that utilizes RS data is better compared to the accuracy of yield estimations derived from the AquaCrop model without the use of RS data.

1.5. Method

An overview of the proposed research method is given in a flowchart in figure 1.5. With reference to figure 1.5, the research method can be further explained as follows.

1. **Data preparation**
    - **RS-data preparation:** In this step temporally-changing estimates of biomass and canopy cover data are made from NDVI time series.
    - **Basic model-data preparation:** AquaCrop requires input data for soil, crop, management and climate. Up to 12 input files are required to run a simulation. These are prepared from existing datasets for the spatial and temporal dimensions of interest.
    - **Validation-data preparation:** Measured yield data for the crops, area and period of interest is prepared for the accuracy assessment.
2. **Modification of AquaCrop**
    In order to force biomass and canopy cover derived from NDVI into AquaCrop, the AquaCrop model is modified. The modification is performed by Prof. D. Raes from the AquaCrop developing team. The communication and evaluation module to interact with AquaCrop is developed by Mr. W. Nieuwenhuis, software developer at ITC.

3. **Yield Estimations**

The simulations are run for area, period and crops of interest, using both the regular and the modified AquaCrop model.

4. **Model accuracy assessment and hypothesis testing**

In this step, the estimated crop yields from both the regular and the modified AquaCrop model simulations, are compared to the field validation data. Basic statistical indicators (X-Y diagram with 1:1 line, correlation coefficient r, determination coefficient R^2 and Nash-Sutcliffe coefficient) are used for accuracy assessment of the model outputs. The result of the model accuracy assessment will establish if the hypothesis has to be rejected or accepted.

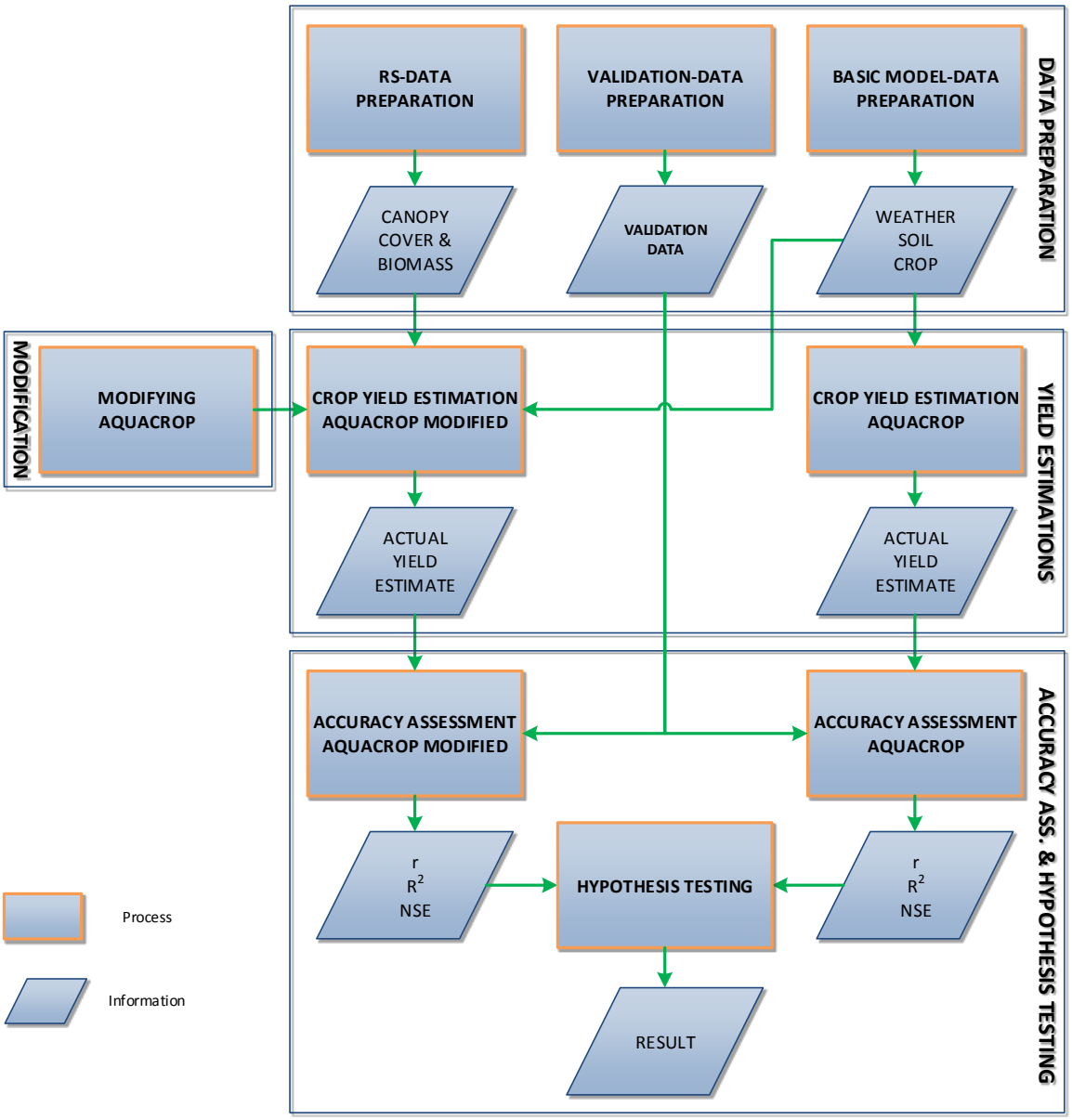

Figure 1.5. Research method flowchart

1.6. Study area

The study area covers the mainland of Spain, located between latitudes 36º and 44º N and longitudes 10º W and 4ºE. It has a total area of around 500.000 km². Figure 1.7 depicts a map of Spain. The dominant climate types in Spain are warm and temperate Mediterranean (Koppen-Geiger: Csa and Csb), cold semi-arid (Koppen-Geiger: Bsk) and temperate oceanic (Koppen-Geiger: Cfb), although other climate types exist in smaller regions. Figure 1.8 shows a Koppen-Geiger climate classification map for Spain (Rubel & Kottek, 2010).

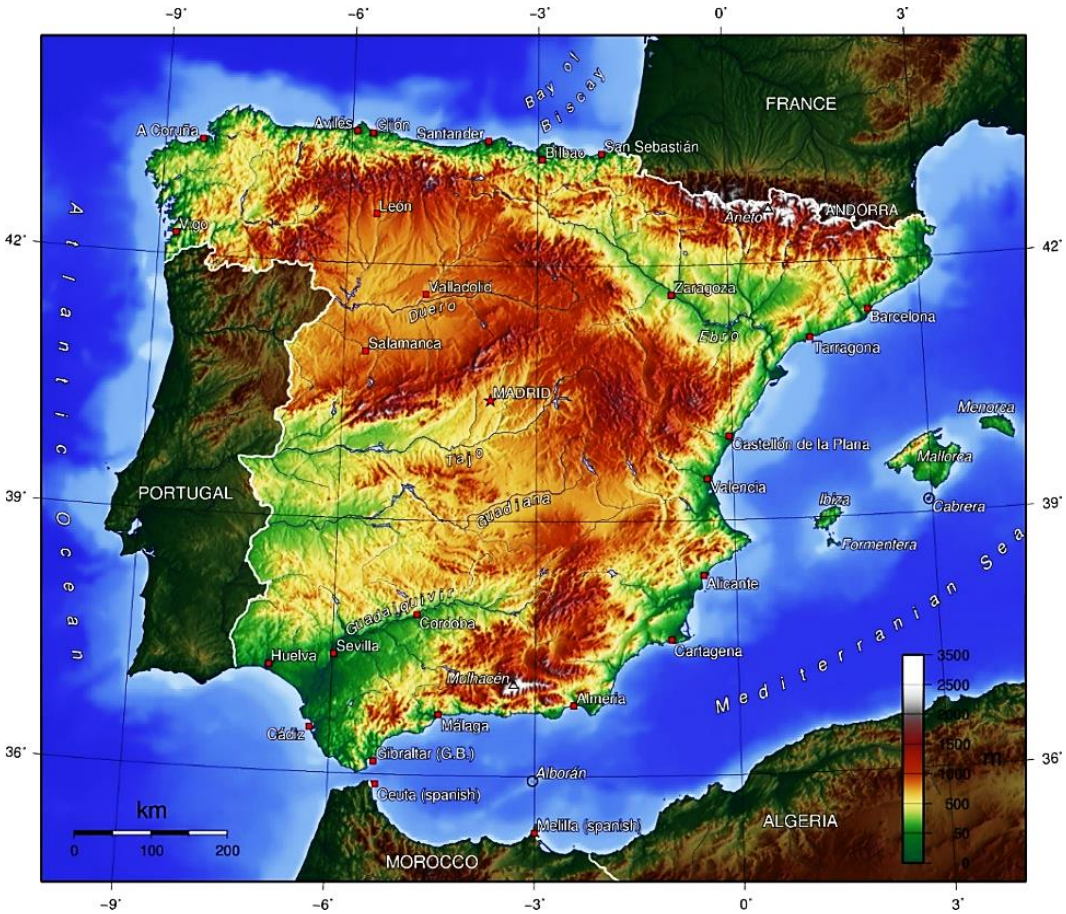

Figure 1.6. Topographic map of Spain (Source: Wikimedia)

Temperature, humidity, sunshine hours and precipitation vary across Spain. For the Mediterranean climate zones, temperatures vary from -15º C in winter to 35º C in summer with annual rainfall exceeding 500 mm. In some regions this can be as much as 2000 mm per year. In the oceanic climate zones, rainfall is abundant, exceeding 1000 mm per year, while temperatures vary only slightly from approximately 9º C to 21º C. The semi-arid climate zones have less rainfall, approximately 300 mm per year and temperatures can exceed 40º C.

According to Eurostat, agriculture accounted for ±2.5% of Spain's Gross Domestic Product and employed approximately 2.2 million people in 2010. Agricultural lands are located across the whole of Spain, with regional variation in crops and absence in the extreme regions i.e. the high mountainous and the very dry areas. Total agriculture lands covered ±24 million hectares of which 26.5% is used for cultivation of cereals, with barley and wheat being the major crops. Table 1.3 details the utilized agricultural area for Spain in 2010. Most of the agriculture area under production is non-irrigated (±80%) and depends solely on rainfall.

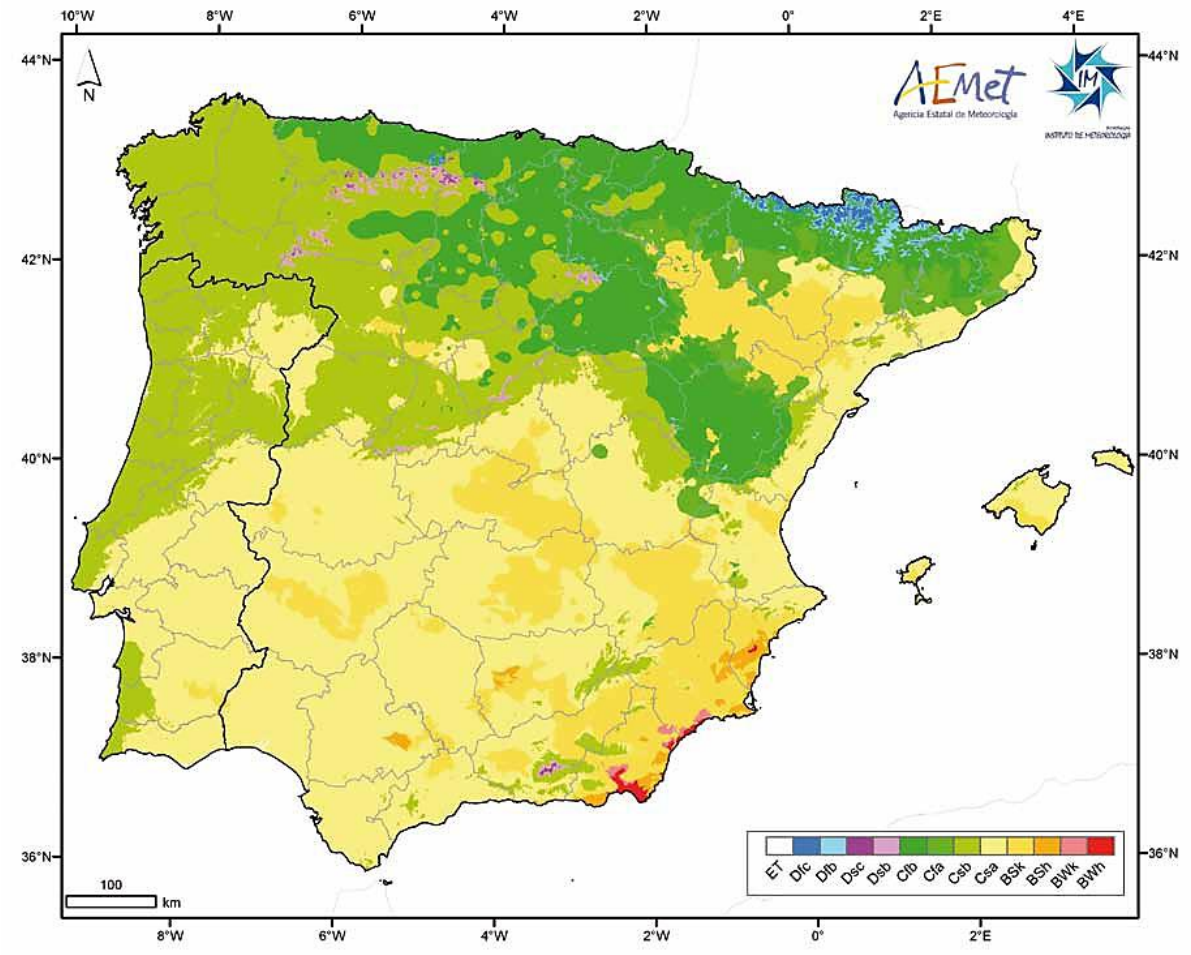

Figure 1.7. Koppen-Geiger climate classification map of the Iberian Peninsula (Source: AEMET)

Table 1.3. Utilized Agricultural Area (UAA) for Spain 2010 (Source: Eurostat)

	Ha	% of UAA
Land use	23,752,690	100.0
Arable land	11,286,010	47.5
Cereals (±34% Wheat, ± 50% Barley)	6,291,820	26.5
Pulses (total)	318,130	1.3
Potatoes	61,890	0.3
Sugar beet	48,580	0.2
Fodder roots and brassicas	17,550	0.1
Industrial crops (total)	900,440	3.8
Fresh vegetables, melons, strawberries	236,490	1.0
Flowers and ornamental plants (total)	6,610	0.0
Fodder crops	736,100	3.1
Seeds and seedlings	4,430	0.0
Other crops on arable land	0	0.0
Fallow land	2,663,960	11.2
Kitchen gardens	3,050	0.0
Permanent grassland and meadow	8,377,390	35.3
Permanent crops	4,086,240	17.2

1.7. Thesis structure

The thesis report is structured as follows. Chapter 1 provided the background, research objective, research questions and hypothesis, a study area description as well as a brief overview of the research method. Chapter 2 details the datasets used and describes the main data pre-processing steps performed. Chapter 3 provides the method used in the research. In chapter 4 the results of the simulations are presented. The discussion is covered in chapter 5, while conclusions and recommendations are given in chapter 6.

2. DATA PREPARATION

2.1. Introduction

This research uses different data from various sources. Distinction is made between the following datasets.

- Validation data: This contains the actual crop area and yield data collected by the Instituto Nacional de Estadística (INE) for Spanish government's annual Agricultural Census program.
- AquaCrop input data: This contains all data required to run the AquaCrop software and is related to the crop and its environment for the temporal and spatial dimensions of interest.
- Remote sensing data: This relates to the two crop features, canopy cover and accumulated aboveground biomass derived from NDVI time series, which will be used to replace or adjust on a daily basis the same crop features simulated in AquaCrop.

Each dataset is treated separately, with provision of details on data sources and carried out data pre-processing.

2.2. Validation data

2.2.1. Validation data selection

The Agricultural Census is an annual statistical operation conducted by the INE since 1962 using the farm as basic unit of information. Its main purpose is to collect, process and disseminate data on the structure of the agricultural sector in Spain. Over 10.000 segments of 700x700m are sampled each census year to collect the required census data. Figure 2.1 shows an overview of the sampling segmentation method.

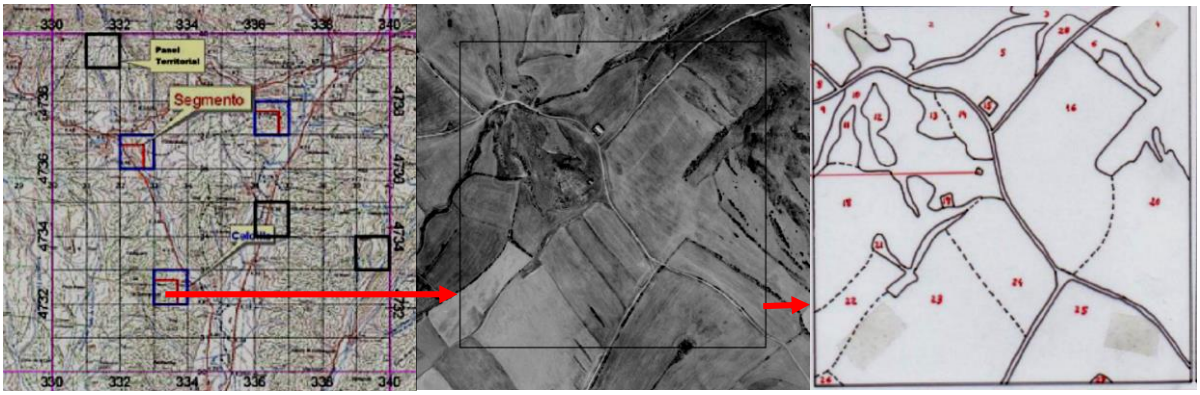

Figure 2.1. Sample segmentation in INE's agricultural census. 700x700m segments are selected from a 1x1km grid and each selected segment is assessed for statistical data of interest. (Adapted from INE)

For this research, INE census data for 2004, 2005, 2006, 2007 and 2009 was made available through the EU's Joint Research Centre (JRC) for all fields within 52.670 segments. Yield data for each field in each segment is determined in different ways.

INE distinguishes the following ways of yield determination:

- Ocular estimation
- Data provided by the farmer
- Determination by combine harvester
- Counting of spikes and grains
- Counting and weighing of spikes
- Weighing of spikes
- Counting and weighing of fruits, counting of trees
- Sectorial determination
- Other

A selection is made for segments containing fields with barley and/or durum wheat, for which the yield has been measured, either by counting spikes and grains, counting and weighing spikes or weighing spikes only. The underlying assumption supporting the selection is that these three methods of measuring the yield are the most accurate. This is assumed because no clear documentation on the remaining acquisition methods could be retrieved. The selection leads to 1323 sample segments, 311 in 2004, 286 in 2005, 257 in 2006, 239 in 2007 and 230 in 2009. These selected segments are treated as sample points and yield data is attributed to the segment midpoint.

2.2.2. Exploratory statistics on validation data

AquaCrop's yield estimations are deterministic and assumed known without error. Although model output is influenced by errors in input data, their relative effect on modelled yield can be investigated by conducting a model sensitivity analysis. In this thesis, only model performance is considered and this is evaluated using the validation data, utilizing linear parametric statistical tools i.e. correlation and linear regression analysis (Moore et al. 2009). For that, the validation data has to be independent, random, and homoscedastic, with the residuals independent and identically distributed (Tedeschi, 2006).

INE uses a grid based stratification setup, based on the CORINE (Coordination of Information on the Environment of the European Environmental Agency) Land Cover map. From 100 km² agricultural land use grid blocks, which are each divided into a mesh of 1 km² cells, three cells are chosen at random in each of the grid blocks. The selected cells always occupy the same relative positions within a block, therefore being uniformly distributed throughout the territory under investigation. The unit of field work is set at a square of 700 by 700 meters attached to the left lower corner of the corresponding 1 km² grid cell. The sample thus obtained is in some cases reinforced with additional segments with the highest cropping intensity. In these cases three more cells are added per block.

From INE's data set over 2004-2009, containing 52.670 segments, the validation data is selected based on crop (barley and durum wheat) and yield measurement method (measured either by counting spikes and grains, counting and weighing spikes or weighing spikes only). Out of 1323 selected sample segments for this research, 695 contain durum wheat fields and 641 contain barley fields. Figure 2.2 shows the histograms for yield and cropped area of the selected sample segments for both crops. The proportion of durum wheat is less than 30% for 75% of selected segments. In case of barley the proportion is less than 13 % for 75% of the selected segments.

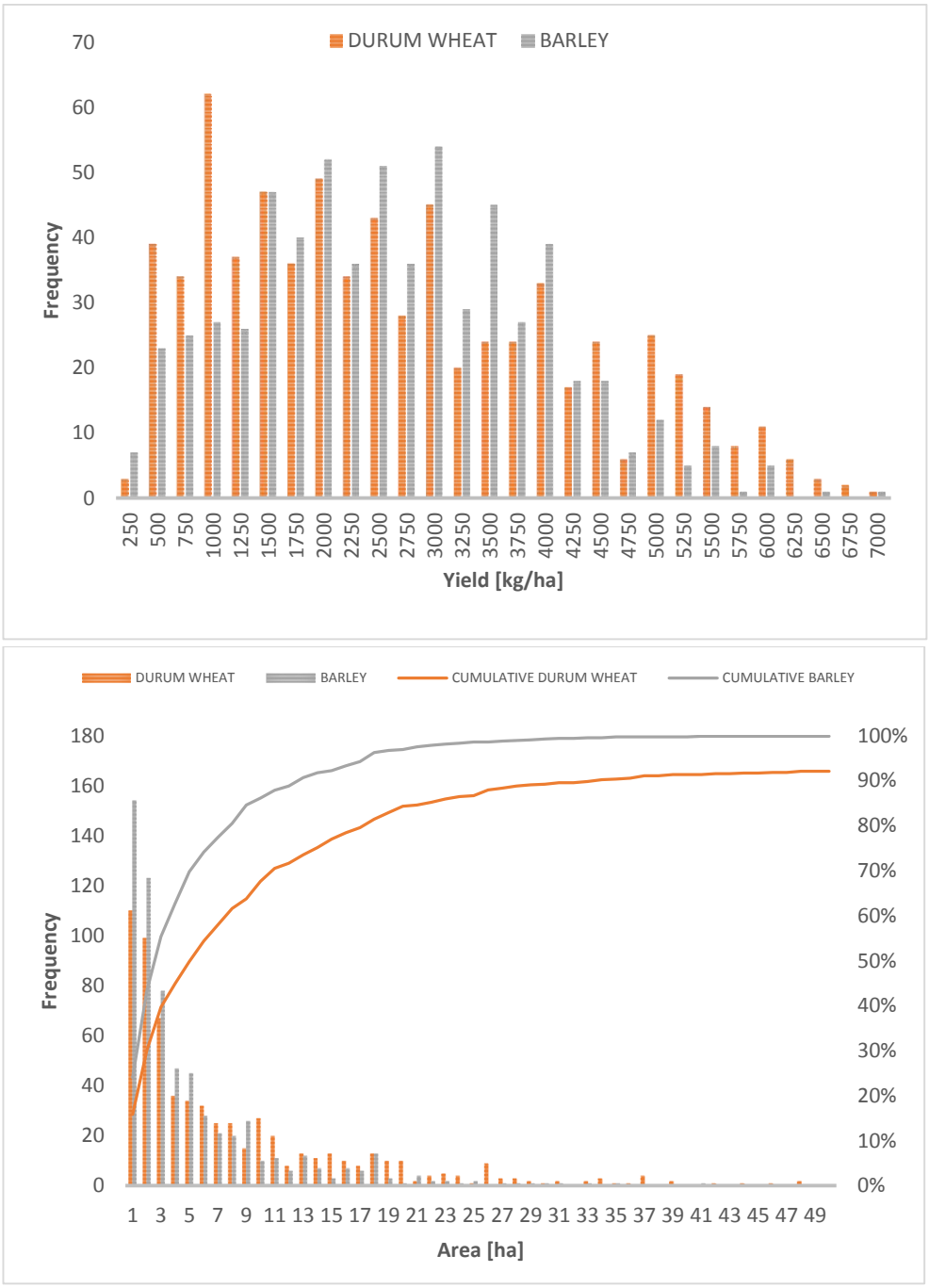

Figure 2.2. Histograms of yield and cropped area for barley and durum wheat for their respective selected sample segments of occurrence (n=695 for durum wheat, n=641 for barley, sample segment area=49ha)

The resulting 1323 segment midpoints (695 for durum wheat and 641 for barley) are superimposed on the crop intensity maps for barley and durum wheat and shown in figure 2.3. The resulting maps as well as the comparison with the climate classification map (see also figures 1.8 and 2.3) support the assumption that validation samples properly represent the variability of the population. Inferences made from the samples are therefore expected to hold.

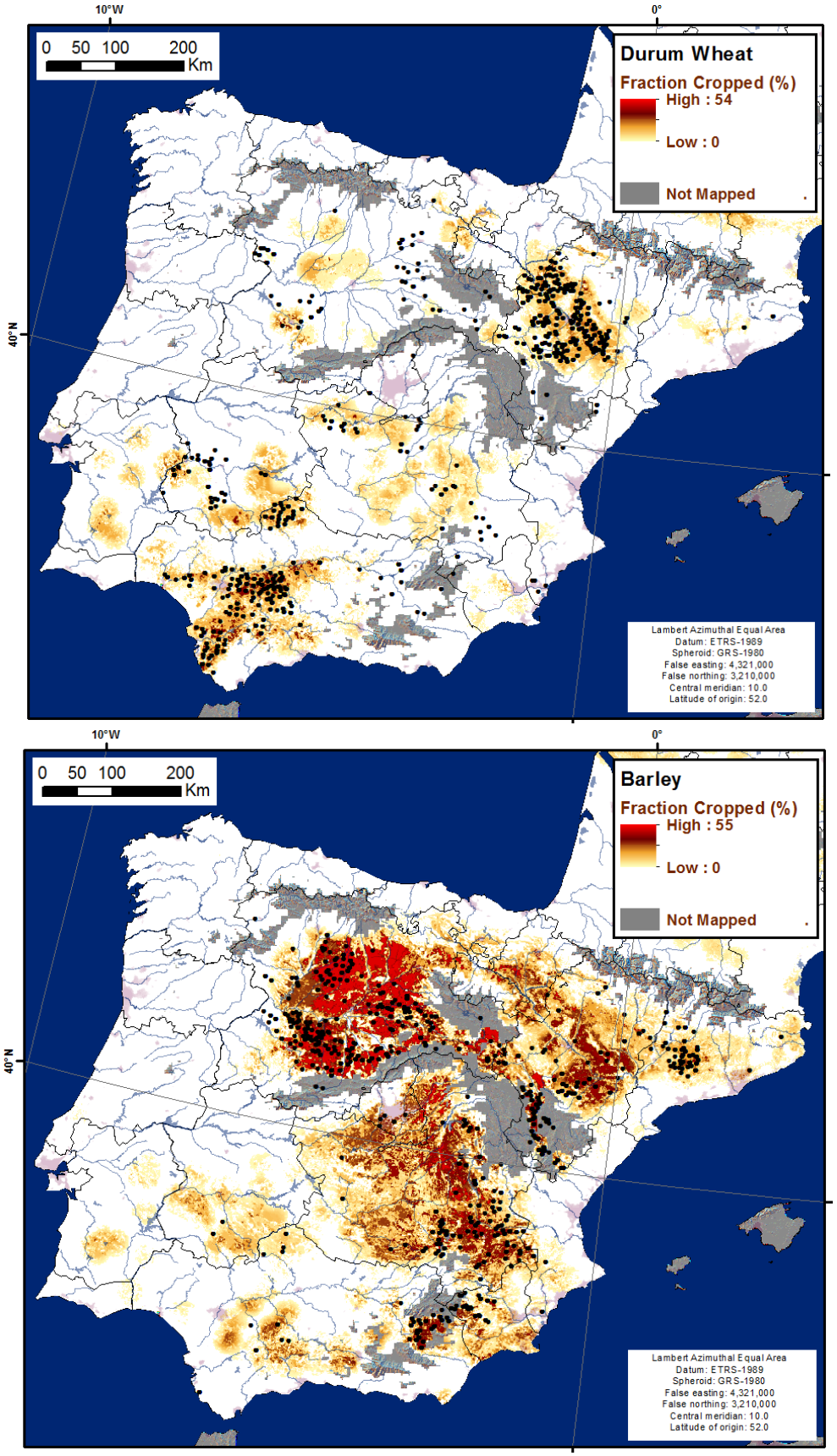

Figure 2.3. Selected segment midpoints for census years 2004-2009 for Durum Wheat (top, n=695) and Barley (bottom, n=641) displayed on top of a crop fraction map (Source: de Bie, 2014)

To verify whether the validation data measurements vary with the relative cropped area in a segment, the standard deviation of the yield is calculated for each selected sample segment containing six or more fields of the respective crop. Both ordinary and weighted linear model relating standard deviation to cropped area in the segment, did not result in significant values for the slopes, hence confirming that no significant relationship exists. Figure 2.4 shows the resulting scatter diagrams with regression lines.

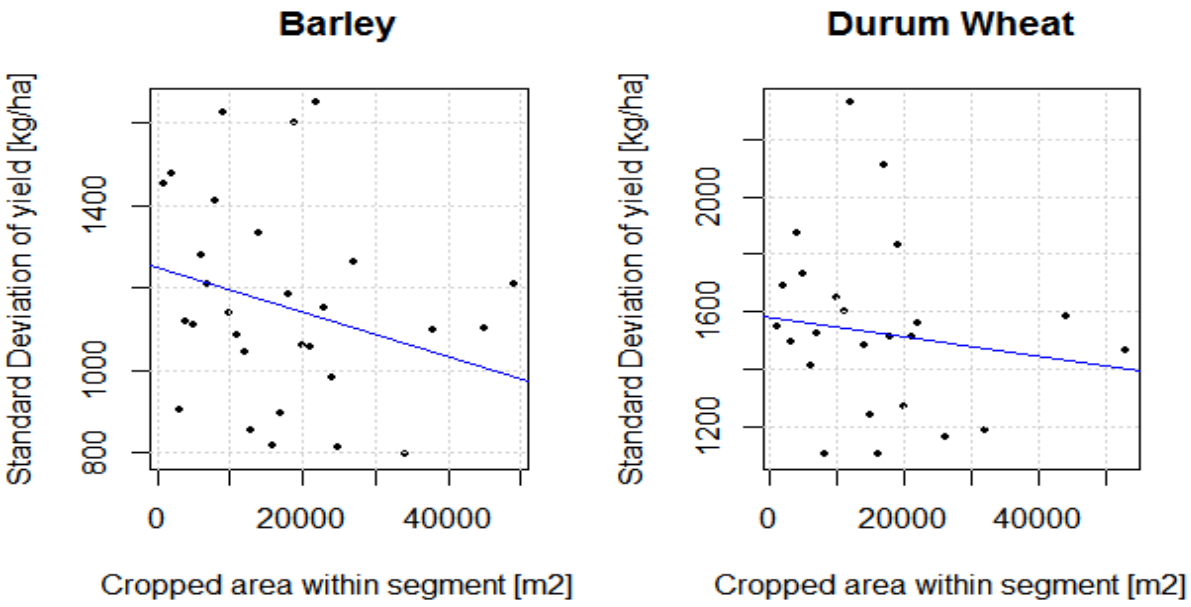

Figure 2.4. Scatter diagrams with linear regression line for the standard deviation of yield of barley and durum wheat with cropped area size

The validation data sets for barley and durum wheat are not normally distributedA Shapiro-Wilks test (Shapiro & Wilk, 1965) performed on the validation data confirms its non-normality (p-values of 8.6e-15 and 2.9e-06 for barley and durum wheat respectively). In order to meet requirements for normality, transformation of validation data is explored using the Box-Cox power transformation method (Box & Cox, 1964). An automated approach, using a readily available function in R software to determine the optimal Box-Cox power transformation (boxcoxnc from R's MASS package) is applied to the data. Unfortunately the optimal power transformed data continues to fail the Shapiro-Wilks normality test (p-values of 1.8e-07 and 0.047 for barley and durum wheat respectively).

Figure 2.5 shows the histograms for original and transformed data. Figure 2.6 shows the QQ-plots for original and transformed data. Even with the validation data or its transformation not perfectly normally distributed, linear regression analysis involving the validation data will still hold if the residuals of the regression are independent and identically distributed or will at least be informative for model comparison (Bennett et al., 2013). The independence and distribution of regression residuals therefore need to be verified when assessing the simulation results.

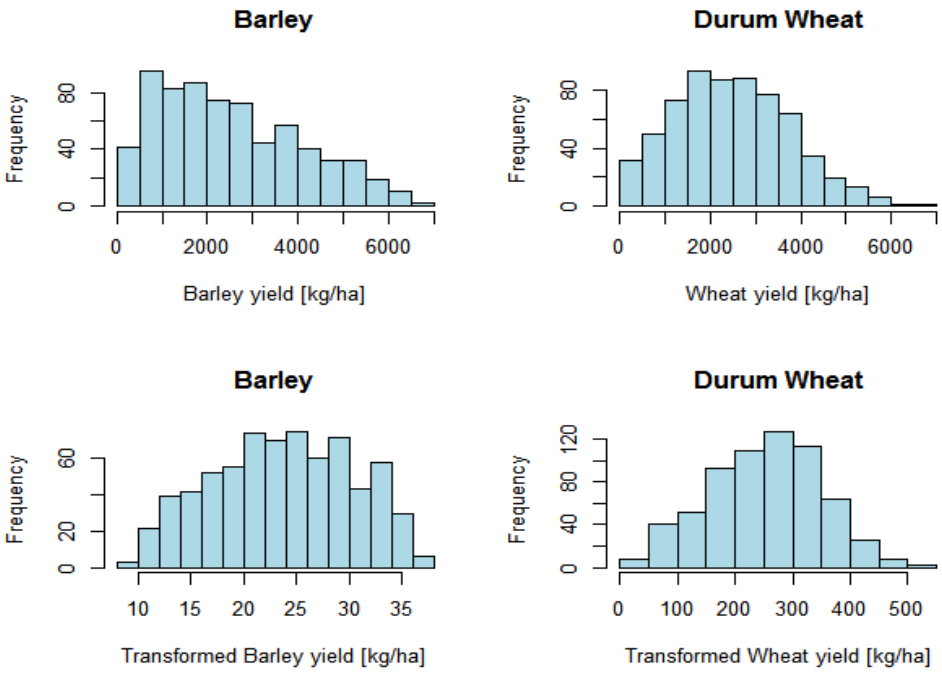

Figure 2.5. Histograms of validation data for barley and durum wheat, original and transformed using optimal BoxCox power transformation (λ=0.41 for Barley, λ=0.71 for durum wheat)

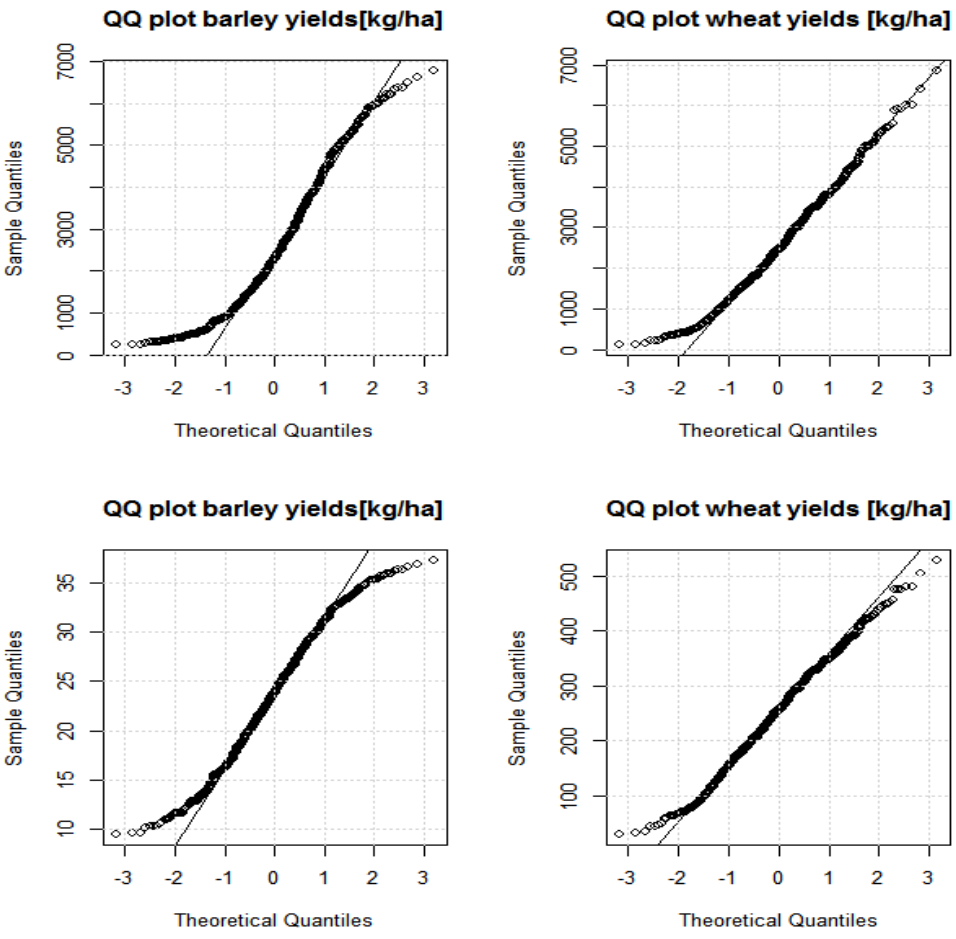

Figure 2.6. QQ-plots of validation data for barley and durum wheat, original (top) and transformed (bottom) using optimal BoxCox power transformation (λ=0.41 for Barley, λ=0.71 for durum wheat)

2.3. AquaCrop input data

2.3.1. Overview of AquaCrop input data

AquaCrop requires specific data related to weather, soil, irrigation, management and crop for each simulation run. Table 2.1 summarizes the input data and specifies the data sources that have been utilized to acquire these. In the following paragraphs, the data types (weather, soil, crop and simulation data) are treated separately.

Table 2.1. Overview of input data for AquaCrop as used in this research

Data type	Description	Sources	Remarks
Weather	Minimum temperature	AEMET	AEMET is the Spanish government's meteorological services agency.
	Maximum temperature		
	Solar radiation		The IRI/LDEO climate database is maintained by the Columbia University in New York USA
	Humidity		
	Wind speed		
	Atmospheric pressure		
	Rainfall	IRI/LDEO Climate Data Library	
	Atmospheric CO_2 concentration	AquaCrop database (Mauna Loa)	AquaCrop contains standard CO_2 concentration records as observed in Mauna Loa, Hawai.
	Reference evapotranspiration	Calculated from weather data using FAO Penman-Monteith equation (FAO, 2012)	
Soil	Horizon thickness	Eurosoils database (EU JRC)	The Soil Geographic Database of Europe (SGDBE) is used.
	Soil water content at:		
	-Field capacity	SEISNET	SEISNET is the Spanish Soil Information System on the Internet.
	-Saturation		
	-Permanent wilting point	AquaCrop Reference Manual	A single horizon is considered with an assumed depth of 3 m. Soils are re-classified based on AquaCrop's own classification system (*Crop yield response to water* 2012)
	Saturated hydraulic conductivity		
	Curve number (runoff determination)		
	Readily evaporable water		
	Capillary rise parameters		
Crop	Crop temperature range	FAO database of calibrated crop files (FAO, 2012).	Calibrated crop files are included in AquaCrop
	Rooting depth		
	Crop stage lengths		
	Canopy growth & decline characteristics		
	Soil water depletion factors		
Simulation	Start & end of crop growing period	Derived from NDVI	Start & end of crop growing period not exactly known, therefore derivation from NDVI
	Start & end of simulation	Start derived from rainfall data, end from NDVI	To start simulation from saturated soil, rainfall events are considered.

2.3.2. Weather data

Weather data, except for precipitation, has been acquired from Spain's national meteorological services agency AEMET. The data is collected as daily observations from approximately 212 weather stations located across Spain. This point dataset has been spatially interpolated to create daily raster datasets for the whole of Spain in order to enable determination of weather parameters at any point. Different spatial interpolation techniques have been considered. Given the extent of the interpolation task, a pragmatic approach using inverse distance weighing (IDW) has been applied to all weather parameters acquired from AEMET. Literature shows (Apaydin et al., 2004; Attorre et al., 2007; Cao et al., 2009; Hofstra et al., 2008; Vicente-Serrano et al., 2003) that this approach provides results with acceptable accuracy, although it may not be the most optimal for each weather parameter under different conditions.

Reference evapotranspiration is calculated using FAO's Penman-Monteith's equation (Allen et al., 1998), given by equation (1).

$$ET_o = \frac{0.408\Delta(R_n - G) + \gamma \frac{900}{T+273} U_2 (e_s - e_a)}{\Delta + \gamma(1 + 0.34U_2)} \quad (1)$$

With: ET_o: reference evapotranspiration [mm day^{-1}]
R_n: net radiation at the crop surface [MJ m^{-2} day^{-1}]
G: soil heat flux density [MJ m^{-2} day^{-1}]
T: mean daily air temperature at 2 m height [°C]
U_2: wind speed at 2 m height [m s^{-1}]
e_s: saturation vapour pressure [kPa]
e_a: actual vapour pressure [kPa]
e_s-e_a: saturation vapour pressure deficit [kPa]
Δ: slope vapour pressure curve [kPa °C^{-1}]
γ: psychrometric constant [kPa °C^{-1}].

For each selected segment midpoint, the weather parameters required to calculate the reference evapotranspiration are acquired from the spatially interpolated raster datasets. Subsequently the reference evapotranspiration is calculated for each selected segment midpoint.

In the case of precipitation data, the IRI/LDEO (International Research Institute for climate & society/ Lamont-Doherty Earth Observatory) climate database has been consulted. This has primarily been done for reasons of efficiency, i.e. it would also have been possible to create precipitation raster data from AEMET's data set, however this is more time consuming and assumed not to lead to improved results. The available precipitation data is created by NOAA (National Oceanic & Atmospheric Administration) based on the CMORPH technique (Joyce et al., 2004). CMORPH combines at a 0.25x0.25 degrees grid resolution 3-hourly precipitation estimates retrieved from several low earth orbiting passive microwave sensor satellite data and geostationary infrared data. In different parts of the world very high levels of accuracy were achieved when validating CMORPH data with ground measurements (Dinku et al., 2008; Dinku et al, 2010). For this research, eight 3-hour estimates have been aggregated into one daily estimate.

2.3.3. Soil data

With regards to the soil data, two soil databases have been explored: the Soil Geographic Database of Eurasia version 4.0 (SGDBE) which is maintained by the EU's Joint Research Centre and Spain's SEISNET (Spanish Soil Information System on the Internet) soil database. The latter provides soil classification data consistent with the United States Department of Agriculture's (USDA) taxonomy (USDA, 2010). SGDBE provides, at a scale of 1:1.000.000, 14 types of attribute data, including soil classification, texture, depth, parent material, soil water regime, impermeable layer and obstacle to roots (Lambert et al., 2003).

As listed in table 2.1, AquaCrop uses a limited set of parameters to characterize up to five soil horizons in a simulation run. Ideally soil parameters are determined in the field before commencing each simulation. Alternatively AquaCrop offers a set of default values for the parameters it uses. Table 2.2 provides an overview of AquaCrop's default values in use. The default parameter values are related to the USDA's soil textural classes. SGDBE however provides soil textural classification based on an EU standard. Figure 2.7 displays the soil textural triangles for both systems.

For this research, an attempt has been made to reclassify the soil for each selected segment midpoint to USDA's standard soil textural classes. This is carried out by combining soil data from both SGDBE and SEISNET. A number of simplifications have been applied. For instance, only one soil horizon is considered with a fixed depth of 3 meters, and this is attributed to the dominant soil type as provided by SGDBE. In addition, no restrictive and impermeable layers have been considered. After the reclassification, AquaCrop's standard soil parameter values have been applied to all selected segment midpoint. The assumption is that with this approach, including its embedded simplifications, at least the minimum requirements for adequate AquaCrop simulations are met (FAO, 2012).

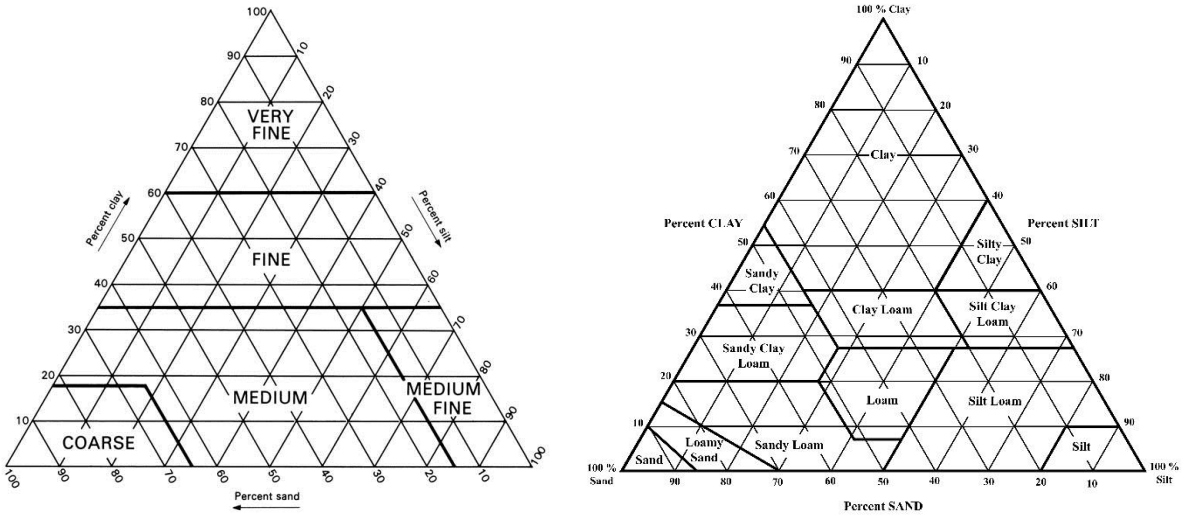

Figure 2.7. Soil textural classes triangle as used in SGDBE (left) and as used in USDA's 12 class-system (right)

(Sources: JRC and USDA)

Table 2.2. Default soil properties values in AquaCrop (Source: AquaCrop Reference Manual)

TEXTURAL CLASS	SOIL WATER CONTENT			SATURATED HYDRAULIC CONDUCTIVITY
	SATURATION	FIELD CAPACITY	PERMANENT WILTING POINT	KSAT
	Vol. %	Vol. %	Vol. %	mm/day
Sand	36	13	6	1500
Loamy sand	38	16	8	800
Sandy loam	41	22	10	500
Loam	46	31	15	250
Silt loam	46	33	13	150
Silt	43	33	9	50
Sandy clay loam	47	32	20	125
Clay loam	50	39	23	100
Silty clay loam	52	44	23	120
Sandy clay	50	39	27	75
Silty clay	54	50	32	15
Clay	55	54	39	2

2.3.4. Crop data

Crop data characterizes the crop under evaluation. Crop parameters describe the crop's growth and development, transpiration, biomass production and yield formation, and response to water and temperature stresses. In addition information is needed on crop stage duration (phenology), planting density, soil rooting and response to soil related stresses. Both barley and durum wheat are grown as winter crops with a dormancy period after germination. For this research, standard calibrated crop files for barley and wheat from the FAO are used. Table 2.3 summarizes the standard crop parameters as used in AquaCrop.

Table 2.3. Crop parameters (*Crop yield response to water* 2012) used in simulation runs

Conservative parameter description	Wheat	Barley
Crop growth & development		
Base temperature (°C)	0	0
Upper temperature (°C)	26	15
Canopy size of average seedling at 90% emergence (cm^2)	1.5	1.5
Canopy growth coefficient (fraction soil cover per day)	0.04902	0.1241
Canopy decline coefficient (fraction soil cover per day)	0.07179	0.07679
Crop transpiration		
Decline of crop coefficient as a result of ageing (%/day)	0.15	0.15
Biomass production and yield formation		
Water productivity normalized (WP*) for ET_o and CO_2 ($gram/m^2$)	15	15
Reduction coefficient on normalized water productivity during yield formation (as % WP*)	100	100
Reference Harvest Index (HI) (%)	48	33
Stresses (Soil-water)		
Upper and lower thresholds of soil water depletion for canopy expansion and shape of curve	0.20/0.65/5.0	0.20/0.65/3.0
Upper threshold of soil-water depletion for stomatal closure and shape of the stress curve	0.65/2.5	0.60/3.0
Upper threshold of soil-water depletion for early senescence and shape of the stress curve	0.7/2.5	0.55/3.0
Upper threshold of soil-water depletion for failure of pollination	0.85	0.85
Possible increase of HI resulting from water stress before flowering (%)	5	5
Coefficient describing positive impact of restricted vegetative growth during yield formation on HI (%)	10	10
Coefficient describing negative impact of stomatal closure during yield formation on HI (%)	7	5
Allowable maximum increase of specified HI (%)	15	15
Anaerobiotic point (for effect of waterlogging on transpiration) (Vol %)	5	15
Stresses (Air temperature)		
Minimum and maximum air temperature below which pollination starts to fail (°C)	5/35	5/35
Minimum growing degrees required for full biomass production (°C-days)	14	14

Table 2.3 continued

None-conservative parameter description	Wheat	Barley
Phenology (cultivar specific)		
Time to flowering or the start of yield formation (Days/°C-days)	127/1250	60/867
Length of the flowering stage (Days/°C-days)	15/200	12/160
Time to start of canopy senescence (Days/°C-days)	158/1700	65/924
Time to maturity (i.e. the length of crop cycle) (Days/°C-days)	197/2400	93/1296
Management dependent		
Plant density (no. of plants/ha)	4500000	1500000
Time to 90% emergence (Days/°C-days)	13/150	7/98
Maximum canopy cover (fraction of soil cover)	0.96	0.8
Soil dependent		
Maximum rooting depth (m)	1.5	1.30
Time to reach maximum rooting depth (Days/°C-days)	93/864	60/854
Soil & management dependent		
Response to soil fertility (%)	50	50
Soil salinity stress (%)	50	50

AquaCrop distinguishes conservative and non-conservative parameters (Raes et al., 2009). Conservative parameters are considered to remain the same under different growing conditions and water regimes. The none-conservative parameters on the other hand, may depend on the cultivar, management practices and location and should be adjusted by the user if possible and as necessary. For this research, exact cultivar en management information is not available and therefore simulations are performed using the standard parameter values as provided in the FAO's calibrated crop files for barley and wheat. The underlying assumption here is that significantly inaccurate parameter values will lead to explicit systematic errors in the model simulation output.

The crop's phenology parameters have been researched in literature, to validate the use of standard parameters in AquaCrop (Abrha et al., 2012; Albrizio et al., 2010; Andarzian et al., 2011; Araya et al., 2010; Isidro et al., 2011; Soddu et al., 2013). Figures from literature regarding the crop's phenology parameters in comparable regions, do not deviate substantially from FAO's standard values. It is therefore considered appropriate to run simulations using the latter. Table 2.4 provides an overview of phenology parameters as found in literature and as provided in the FAO's calibrated crop files for barley and wheat.

Table 2.4. Crop phenology parameters from literature and as used in AquaCrop.

	Parameter description	AquaCrop	Isidro *et al.* (2011) [Spain]**	Soddu *et al.* (2013) [Sardinia, Italy]	Andarzian *et al.* (2011)*** [Ahvaz, Iran]
DURUM WHEAT	Time to flowering	127 (1250)*	(1149-1445)	145	93 (1277)
	Length flowering stage	15 (200)	(189.5-235)	10	10 (140)
	Time to senescence	158 (1700)	(1340-1680)	155	100 (1372)
	Time to maturity	197 (2400)	(1978-2274)	194	142 (2040)

		AquaCrop	Araya *et al.* (2010) [Mekelle, Ethiopia]	Abrha *et al.* (2012) [Mekelle, Dejen & Maiquinha, Ethiopia] [Bari, Italy] [Breda, Syria] [Montana, USA]
BARLEY	Time to flowering	60 (867)	(676)	(696-940)
	Length flowering stage	12 (160)	(130)	(160-180)
	Time to senescence	65 (924)	(962)	(704-1063)
	Time to maturity	93 (1296)	(1105)	(1069-1520)

*:Units: Days (°C-days) **:[Study Area] ***: Study refers to Bread Wheat

2.3.5. Simulation dates

Simulation dates relate to the start and end of each simulation and the start and end of each crop growing period (CGP) for the site under simulation. AquaCrop requires the user to specify these four dates for each simulation run. The proper order of these dates is: start of simulation, start of CGP, end of CGP, end of simulation, although AquaCrop also allows the simulation start to be after the start of CGP.

To determine these dates for each simulation, the following logic has been applied. For each simulation, the start and end of CGP has been determined utilizing crop calendars and hyper temporal NDVI data. The end of simulation date is then set at the latest occurrence of the end of CGP date per for each season. The start of simulation is set at the date in September or October prior to the start of CGP, with the maximum rainfall occurring. This sets the initial timing for AquaCrop's soil water balance simulation, from which the crop growth simulation further develops. For simulations where a starting point cannot be determined based on prior rainfall events, rainfall events after, but close to the start of CGP (in September or October) are considered.

From crop calendars provided by the USDA (2012) we can derive the months for CGP start and end for durum wheat and barley in Spain. This information is further complemented with regional crop calendars derived in previous research (Khan, 2011; Supit & Wagner, 1999). In general, both crops are planted in November and harvested in June. However, rather than a month, AquaCrop requires a specific date for both start and end of CGP. Because this information is not available at field level, one way to determine this is from remote sensing data i.e. from NDVI-profiles. The concept behind this idea is best explained using figure 2.8.

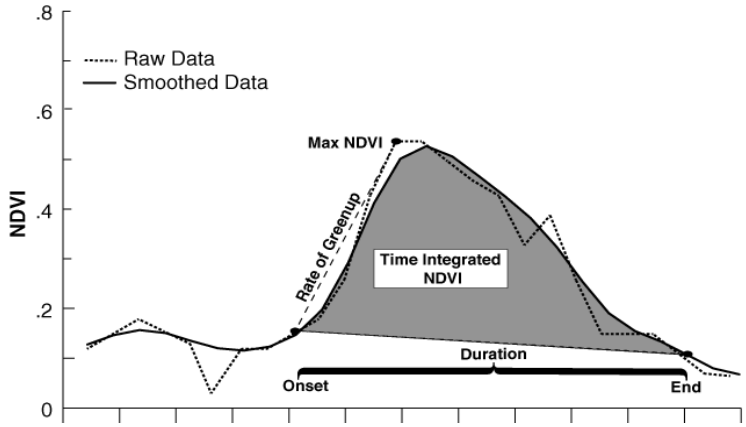

Figure 2.8. Agro-phenology indicators derived from an NDVI curve. The x-axis represents the 12 months of a season. (Reed et al., 1994)

From the NDVI curve given in figure 2.8, three key phenology indicators can be derived: onset of greenness, maximum NDVI and end of greenness. In the case of spatial homogeneity, where one NDVI pixel represents a single crop planted approximately at the same time, the onset of greenness can confidently be related to the start of CGP and the end of greenness to the end of the CGP. For more spatially heterogeneous pixels, this association does not necessarily hold, however the same approach may still be used. Different techniques are used to determine onset and end of greenness from NDVI. Curnel and Oger (2006) describe techniques based on thresholds, moving averages, first derivatives and empirical equations. They conclude that although none of these techniques is ideal, they are still useful depending on context and objectives. For this research, start of the crop growing period and end of the crop growing period are determined for each simulation based on a delayed moving average method (Reed et al., 1994). Here, a moving average is calculated for each NDVI curve, creating a new series with a time lag. The actual NDVI values are compared to the calculated moving average series and a trend change can then be distinguished. Trend changes represent the start and the end of the crop growing period. To determine the trend changes, a window of thirteen 10-day periods (SPOT-NDVI Maximum Value Composites) was used to calculate the moving average. This conforms to recommendations from literature (Beurs & Henebry, 2010; Reed et al. 1994).

Figure 2.9 illustrates the applied method to derive start of the crop growing period utilizing a delayed moving average. The end of the crop growing period is determined similarly, however by applying the moving average in inverse order (Beurs & Henebry, 2010; Reed et al., 1994). Table 2.5 summarizes main statistical characteristics of the resulting simulation and cropping dates.

Table 2.5. Means, 25th & 75th percentiles of start, end and length of crop growing period calculated from selected segments.

	2004	2005	2006	2007	2009
Start CGP mean	9-Nov-03	16-Dec-04	2-Nov-05	27-Oct-06	26-Nov-08
End CGP mean	17-Jun-04	21-Jun-05	19-Jun-06	12-Jun-07	5-Jun-09
Length CGP mean	221 days	187 days	229 days	228 days	191 days
Start CGP 25th percentile	20-Oct-03	10-Nov-04	10-Oct-05	10-Oct-06	20-Oct-08
Start CGP 75th percentile	20-Nov-03	10-Jan-05	10-Nov-05	31-Oct-06	20-Dec-08
End CGP 25th percentile	30-May-04	31-May-05	20-May-06	31-May-07	10-May-09
End CGP 75th percentile	30-Jun-04	30-Jun-05	20-Jun-06	20-Jun-07	10-Jun-09
Length CGP 25th percentile	203 days	161 days	202 days	202 days	171 days
Length CGP 75th percentile	244 days	212 days	233 days	243 days	212 days

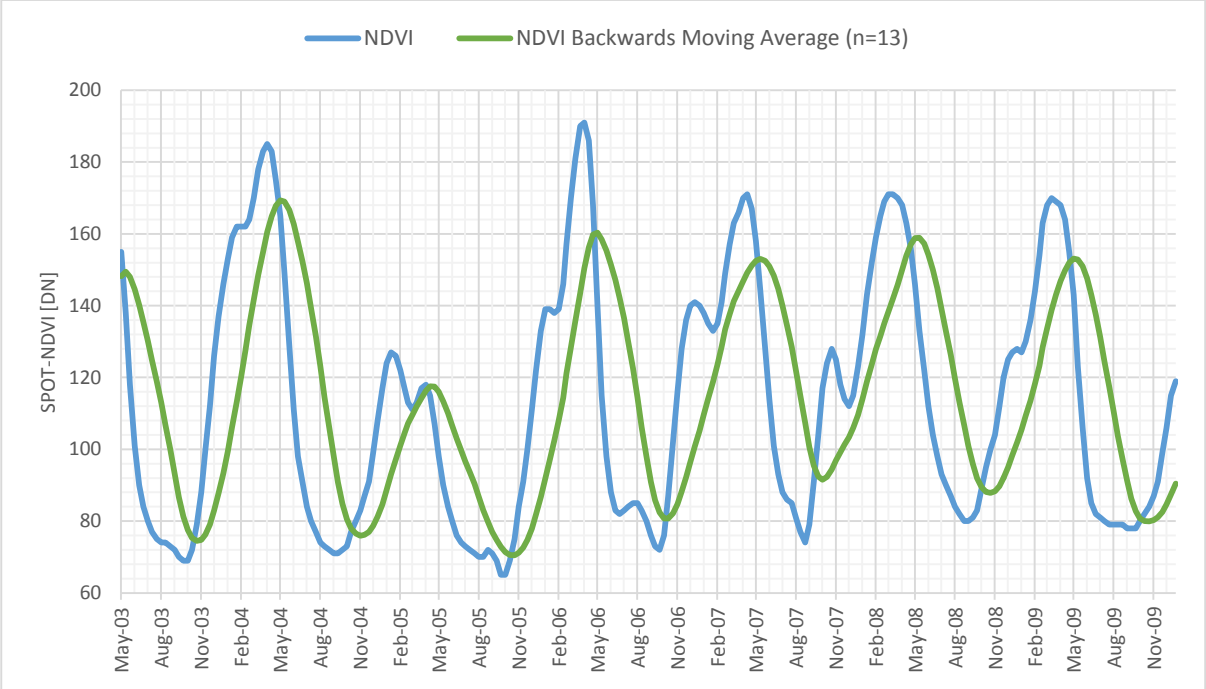

Figure 2.9. Illustration of start of CGP detection based on a delayed moving average method (Reed et al., 1994) CGP start is where upwards moving NDVI crosses the Moving Average curve.

The actual CGP start and end dates for each selected segment are not known. However, the average resulting dates retrieved from the NDVI profiles, comply with findings from literature (Khan, 2011; Supit & Wagner, 1999). The relatively late average start of CGP in 2005 may be attributed to the drought that Spain suffered during that specific season (European Drought Centre). Figure 2.10 illustrates how canopy cover development in a simulation run is expected to relate to simulation start, start of CGP and end of CGP. The figure therefore displays NDVI, its trend changes used to determine start of CGP and end of CGP and the rainfall maximum before the start of CGP which is used to set the start of simulation.

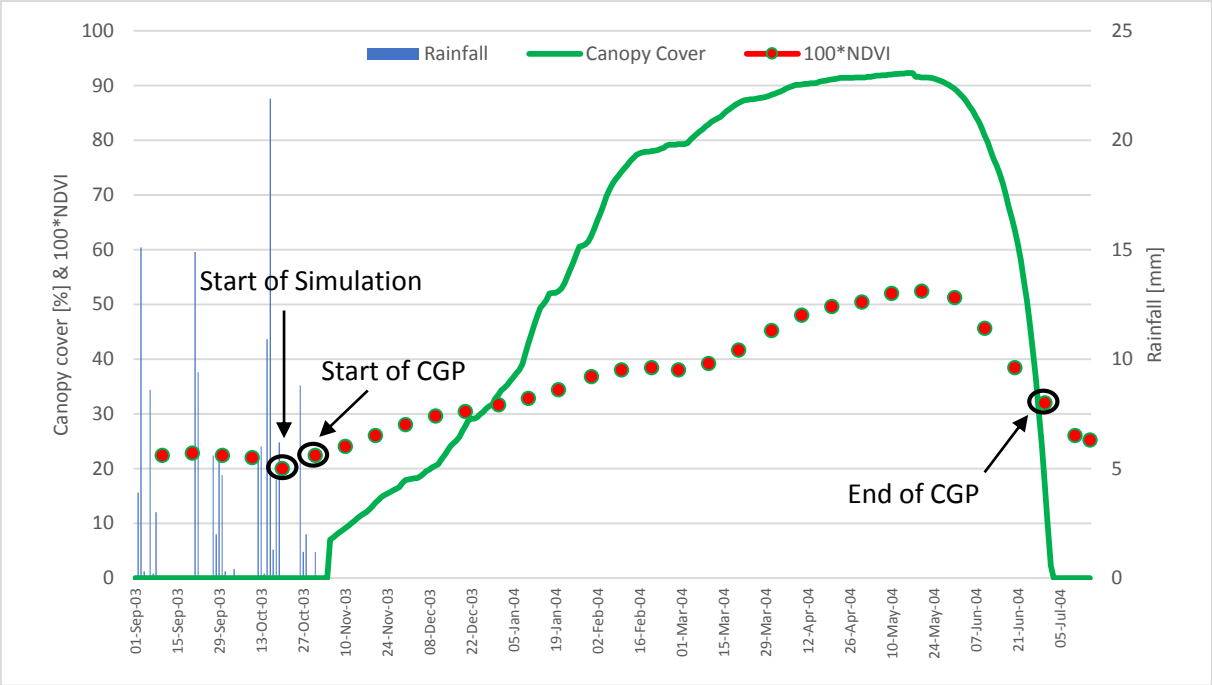

Figure 2.10. Illustration of determination of Simulation start, start of CGP and end of CGP for an imaginary sample site and their relationship with expected canopy cover development. NDVI is scaled for display purposes. Rain data is only shown prior to start of CGP

2.4. Remote sensing data

2.4.1. Normalized Difference Vegetation Index (NDVI) time series

The Normalized Difference Vegetation Index or NDVI is a dimensionless index that represents the photosynthetic activity in vegetation. NDVI is acquired by applying the formula NDVI = (NIR - RED)/(NIR + RED), where NIR is the near-infrared reflectance and RED is the (visible) red reflectance, reflected by vegetation and captured by (satellite) sensors. NDVI values vary from -1 to 1 whereby values close to zero correspond to an absence of green vegetation and negative values in principle occur only over water surfaces. NDVI can be calculated from different sensors, however for this research only coarse resolution NDVI time series are considered and referred to.

In numerous studies NDVI has been related to different plant attributes like plant photosynthetic activity and plant productivity. This is quite extensively summarized, along with associated shortcomings, by Pettorelli *et al.* (2006) and Santin-Janin *et al.* (2009). Noise in NDVI data is mainly due to cloud cover, water, snow or shadow, and usually leads to decreased NDVI values. Different smoothing techniques may be used to properly handle noise (Pettorelli et al., 2006). A commonly used method is maximum value composition (MVC) whereby NDVI values are aggregated and the highest NDVI value for period and area considered is retained.

NDVI is capable of capturing the specific periodic behaviour that crops exhibit. The relationship between NDVI and biomass is known to saturate at high biomass values and high vegetation densities (Gitelson, 2004; Santin-Janin et al., 2009). The reflectance of RED can be attributed to one layer of leafs while the NIR reflectance results from multiple layers of leafs dues to the high transmittance of NIR radiation through green leafs. As a consequence, RED saturates faster, leading to saturation of NDVI where the Leaf Area Index (the one-sided green leaf area per unit ground surface area) becomes larger than 3. In Spain, barley and durum wheat are mostly grown under water limiting conditions leading to low yield potentials (FAO,

2012). For environments with low and medium yield potential, LAI values are usually lower than 3 (Aparicio et al. 2000), and therefore the assumption that NDVI saturation has little relevance for this research seems justified. Other pitfalls concerning NDVI, relate to mixed pixels, misregistration, and the quality of the information in respect to spatial location (Pettorelli et al., 2006).

Despite the limitations, there are a number of reasons why coarse resolution NDVI time series have been chosen in this research. Firstly, coarse resolution NDVI time series are readily available at zero cost to researchers. Secondly, the use of coarse resolution NDVI time series (and similar vegetation indices) is currently the only feasible approach when analysing vegetation considering the scale and limitations of this research. Thirdly, crop characteristics (i.e. LAI, fractional cover) derived from coarse resolution NDVI time series have proven to be useful over time (Glenn et al., 2008).

The NDVI data used is the 10-day maximum value composite georeferenced 1x1 km product derived from the Système pour l'Observation de la Terre (SPOT) vegetation program (Maisongrande et al., 2004). SPOT uses a RED band (0.61-0.68µm) and a NIR band (0.78-0.89µm) to calculate NDVI. NDVI is made available as an unsigned 8 bit integer digital number (DN) in accordance with the formula: DN = (NDVI+0.1)/0.004. This converts the NDVI value of -1 to 1 to a DN of 0 to 255. For each month, three products are created for each pixel, leading to 36 images for a year. The SPOT NDVI time series have been cleaned, by removal of invalid pixels based on accompanying quality records, and upper envelope filtered utilizing a Savitsky-Golay filtering technique (Chen et al., 2004). This technique smooths out noise in the NDVI time series caused primarily by cloud contaminiation and atmosperic variability, which usually depress the NDVI values. The cleaning and filtering was performed by Dr. de Bie and the resulting NDVI-time series were made available for this research. The used data set comprises 2003-2009, a total of 252 images, and cover the whole of Spain.

2.4.2. Derivation of canopy cover from NDVI

From the upper envelope filtered NDVI series the canopy cover (also known as fractional vegetation cover) is derived. Canopy cover is the fraction of soil surface covered by green canopy, considering a vertical projection of the shoot (or crown) area of the vegetation. The concept of canopy cover is displayed in figure 2.11.

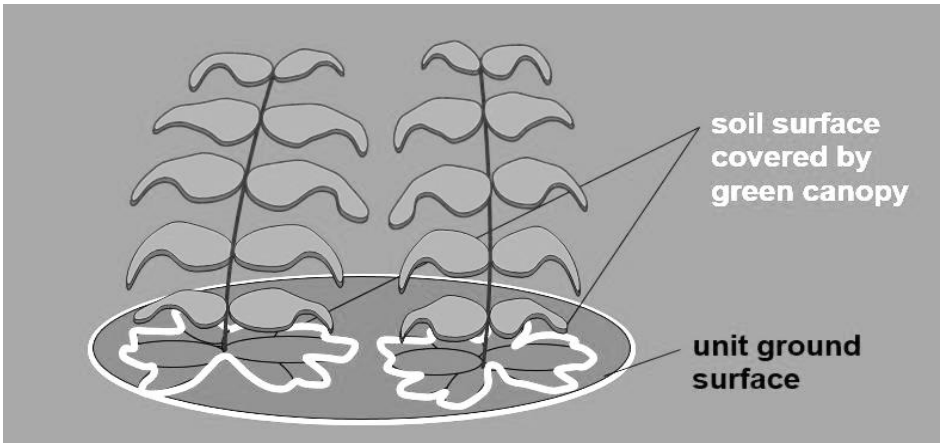

Figure 2.11. Canopy cover (CC) or vegetation fraction illustrated. CC is the fraction of soil surface covered by green canopy (Source: AquaCrop training material, Raes 2012)

Canopy cover is used in AquaCrop to model the water flux at the surface. In this way, the separation of evapotranspiration into productive water use (i.e. crop transpiration) and soil evaporation can be achieved (Raes et al., 2009).

Different approaches exist to derive canopy cover from NDVI (Jiang et al., 2006). For this research, two approaches are considered. Firstly canopy cover is derived using the scaled NDVI approach of Gutman and Ignatov (1998). They suggest that the canopy cover in a dense vegetation mosaic (patchy structured) pixel, can be derived using equation (2).

$$CC = \frac{NDVI - NDVI_S}{NDVI_\infty - NDVI_S} \quad (2)$$

With: CC the canopy cover
NDVI the NDVI for the pixel under evaluation
$NDVI_S$ the NDVI for bare soil
$NDVI_\infty$ the NDVI for dense green vegetation

The vegetation density varies over the crop's growing season, and consequently Gutman and Ignatov's dense vegetation mosaic pixel model may not be an accurate proxy for canopy cover throughout the growing season. Gutman and Ignatov argue however that even in case of non-dense vegetation mosaic pixels where the Leaf Area Index exceeds 3, the above formula will hold (Gutman & Ignatov, 1998). The sample segments under evaluation, have a mosaic structure, as can be seen in the example displayed in figure 2.1. Alternatively the canopy cover is also derived from a generic relationship as proposed by Baret *et al.* (1995). Their approach links the vertical gap fraction, which is the fraction of soil seen from nadir, to the canopy cover as given in equation (3) and (4).

$$CC = 1 - P_0 \quad (3)$$

where

$$P_0 = \left(\frac{NDVI_\infty - NDVI}{NDVI_\infty - NDVI_S} \right)^{0.6175} \quad (4)$$

With: CC the canopy cover
P_0 the vertical gap fraction
NDVI the NDVI for the pixel under evaluation
$NDVI_S$ the NDVI for bare soil
$NDVI_\infty$ the NDVI for dense vegetation

In an analytic study by Jiang *et al.* (2006) comparing canopy cover retrieval from NDVI using different methods for developing cotton canopy over a variety of soil backgrounds and for both wet and dry soil conditions, the model of Baret *et al.* performed somewhat better than Gutman and Ignatov's. For this research both will be utilized and results will be compared to AquaCrop's baseline output (without forcing of CC) to determine which performs best.

Establishing values for $NDVI_S$ and $NDVI_\infty$ is considered difficult and uncertain (Liu et al., 2012) due to the dependence on soil type, vegetation type, atmospheric factors and leaf properties. Different approaches are suggested in literature. Gutman and Ignatov (1998) use constants, independent of location and vegetation, while Zeng *et al.* (2000) derive $NDVI_\infty$ for each land cover class separately. Alternatively logistic modelling is utilized to derive values for $NDVI_S$ and $NDVI_\infty$ (Liu et al., 2012) and even NDVI histograms (Jimenez-Munoz et al., 2009). In this research, the values for $NDVI_S$ and $NDVI_\infty$ are estimated separately for barley and durum wheat. The assumption is that if $NDVI_S$ and $NDVI_\infty$ are crop specific, the resulting CC will be crop specific. Out of 1323 selected sample segments for this research, 695 contain durum wheat fields and 641 contain barley fields. Only 13 selected sample segments contain both.

The minimum and maximum value of NDVI for each of the 1323 selected segment midpoint over 2004-2009 is determined by sampling the NDVI dataset for the selected sample segment midpoints. The NDVI values are then attributed to barley, durum wheat or both, depending on which of the crops occurs in the corresponding sample segment. Figure 2.12 shows the histograms for minimum and maximum value of NDVI for both crops.

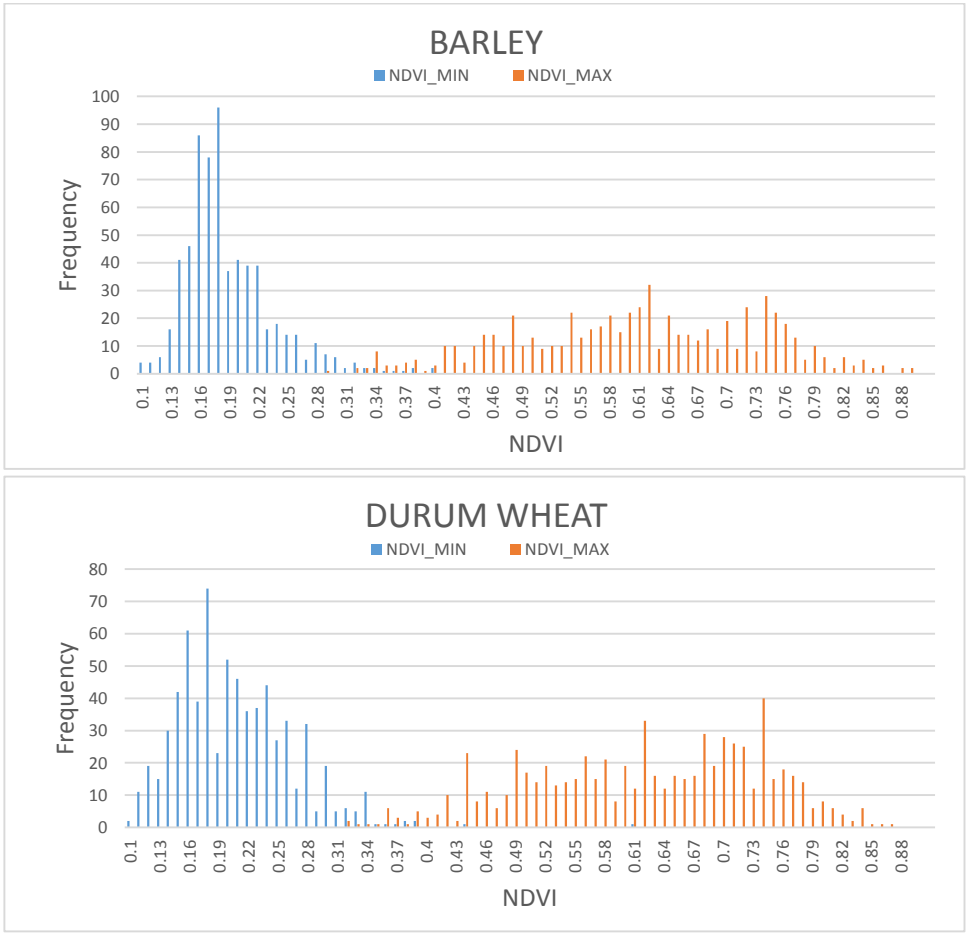

Figure 2.12. Histograms of NDVI minima and maxima for barley and durum wheat for their respective selected sample segments of occurrence (n=695 for durum wheat, n=641 for barley)

The NDVI is based on reflectances in RED and NIR averaged over the pixel area. The contribution of a crop's reflectances towards NDVI is therefore relative to its fractional size in the pixel. To estimate the values for $NDVI_S$ and $NDVI_\infty$ separately for barley and durum wheat, some simplifications have been applied. It is assumed that the NDVI values sampled for all 1323 sample segment midpoints represents the NDVI of the sample segment. In fact, not only is there a discrepancy between sample segment size (700x700m) and NDVI pixel size (1x1km), it is also possible to have one sample segment fall within multiple adjacent NDVI pixels. In addition, by calculating NDVI minima and maxima over 2004-2009, variations across seasons are not considered. It is also implicitly assumed that crop fractions throughout this period remain approximately the same. These factors which are likely to introduce inaccuracies are acknowledged but not considered further. We assume from now on that the contribution of a crop field's reflectances towards the NDVI determined at the sample segment midpoint, is relative to its fractional size in the sample segment for the season under consideration. A weighted sum of the contribution values is then calculated, where the weights are set equal to the relative fraction of the crop in a selected sample segment. Table 2.6 summarizes the values for $NDVI_S$ and $NDVI_\infty$ determined for each crop.

Table 2.6. Values for $NDVI_S$ and $NDVI_\infty$ as determined for barley and durum wheat

	$NDVI_S$	$NDVI_\infty$
Barley	0.17	0.59
Durum Wheat	0.18	0.63

By applying the determined values for in $NDVI_S$ and $NDVI_\infty$ for each crop separately in Gutman and Ignatov's dense vegetation mosaic pixel model and Baret *et al.*'s gap fraction model, the canopy cover for each selected sample segment midpoint can be calculated by crop. To avoid negative values and values over 1, both model outputs are truncated between 0 and 1. Figure 2.13 shows a random selection of calculated canopy cover curves based on Gutman and Ignatov's model for the 2003-2004 season for durum wheat and the same selection of calculated canopy cover curves based on Baret *et al.*'s model.

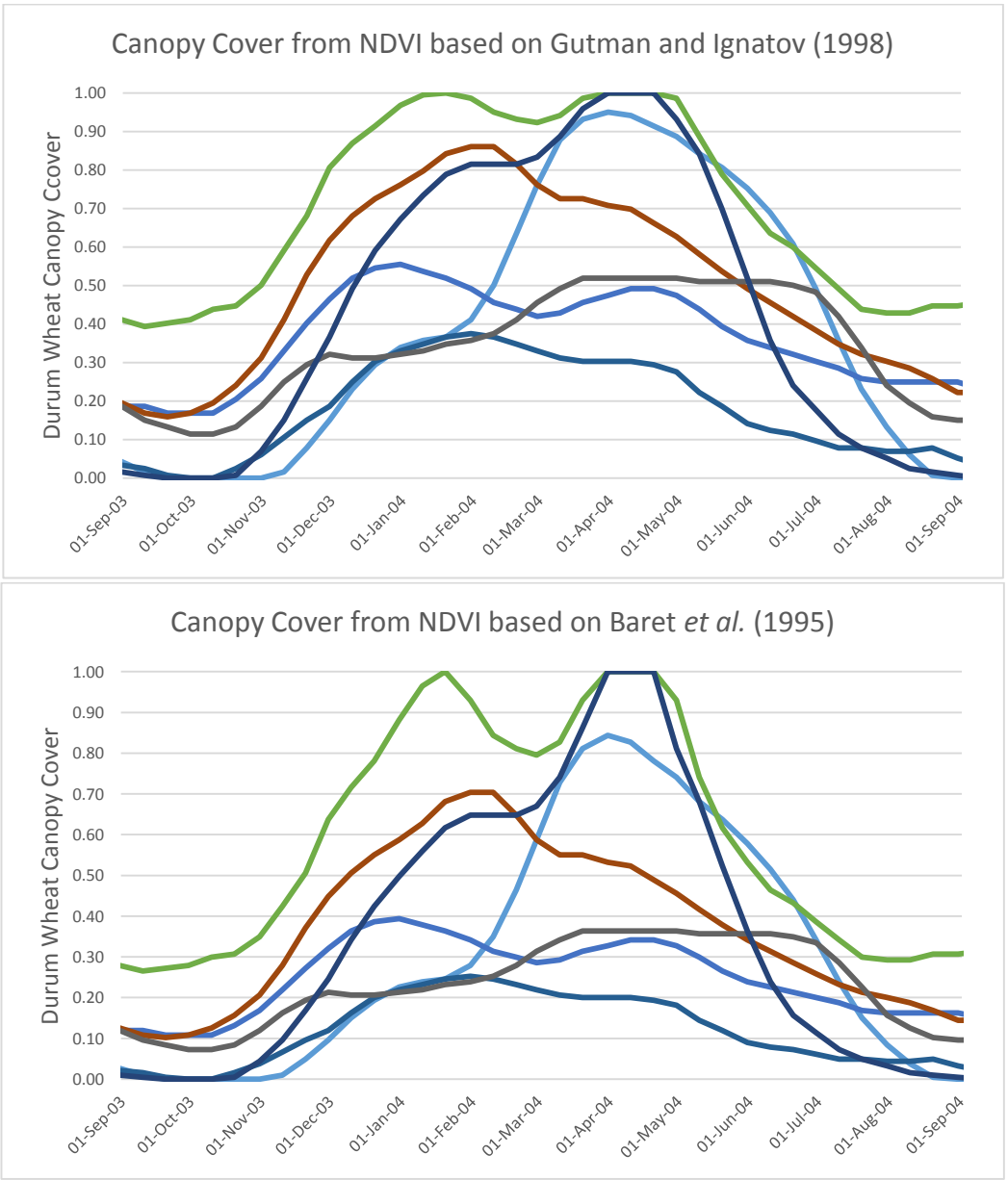

Figure 2.13. Durum wheat canopy cover curves for some sample segment midpoints in the 2003-2004 season, as derived from NDVI using Gutman and Ignatov's (1998) dense vegetation mosaic pixel model and using Baret *et al.*'s gap fraction model.

For AquaCrop simulations, data is required on a daily, 10-daily or monthly basis. For this research, daily data is used. The daily data series with regards to canopy cover are derived from the canopy cover data by means of linear interpolation. The linear interpolation is performed using R software.

2.4.3. Derivation of biomass from NDVI

NDVI has been used as a proxy for plant biomass in many studies. By establishing the correlation between different spectral indices and wheat biomass in different phonological stages, Bao *et al.* (2008) conclude that correlation between biomass and NDVI is phonological stage dependant. Especially in the later stages of crop development (i.e. flowering and grain-filling) very low correlations exist. Another interesting approach is the use of Time Integrated NDVI (TINDVI). TINDVI is the area under the NDVI curve calculated from start-to-end of the season. Figure 2.8 displays the concept of TINDVI. Calera *et al.* (2004) distinguish empirical relationships between biomass and a vegetation index, and the use of models based on Absorbed Photosynthetic Active Radiation (APAR). Both relationships indicate that a linear relationship between the TINDVI and biomass exists. Care has been suggested with regards to the use of cumulated variables in growth models (Malet et al., 1997), since the relationship between two time-accumulated variables (i.e. biomass and TINDVI) may just be a meaningless artefact, because the apparent relationship may be present only due to the fact that both variables increase with time. Calera *et al.* (2004) do conclude that despite this pitfall, good agreement is established for barley and maize, utilizing a linear relationship between TINDVI and biomass.

For the purpose of this research, a linear relationship between biomass and TINDVI is investigated. From the smoothed SPOT NDVI series, daily NDVI values are interpolated utilizing R software. From start to end of the season these NDVI values are summed for each selected sample midpoint using the CGP and simulation dates as acquired in section 2.3.4. Biomass is calculated from INE's sample yield records utilizing a fixed harvest index (HI) derived from literature. Because the HI is defined as the ratio of yield to aboveground biomass, biomass may be retrieved from yield by dividing yield by HI. Royo *et al.* (2007) report a mean value of 0.41 for the HI of modern durum wheat cultivars used in Spain. Albrizio *et al.* (2010) reported a HI of 0.41-0.45 for winter barley during a three season research experiment (2005-2008) in Bari, Italy. To derive biomass from yield records, a harvest index of 0.41 and 0.43 will be utilized for durum wheat and barley respectively. In reality HI for a specific crop varies with cultivar, environmental conditions and agricultural management practices as becomes apparent in many different studies (Cantero-Martínez et al., 2003; Royo et al., 2004; Villegas et al., 2001).

A weighted linear regression is established for both barley and durum wheat. The weights are calculated with equation (5).

$$\text{weight of crop i in sample segment j} = \frac{\text{area of crop i in sample segment j}}{\text{total area of segment j}} \quad (5)$$

By applying weights, more importance is given to sample segments with higher relative crop cover. It is assumed that the relationship between NDVI data and crop biomass improves if the relative crop cover in a pixel increases.

The results are presented in figure 2.14. The linear regression leads to an R^2 of 0.19 for barley and 0.14 for durum wheat with significant p-values for slope and intercept. Building linear models for separate seasons as suggested by Diouf and Lambin (2001) did not lead to improved results. From the linear models, daily values of biomass are calculated for each selected sample midpoint and used in the RS forced simulation runs.

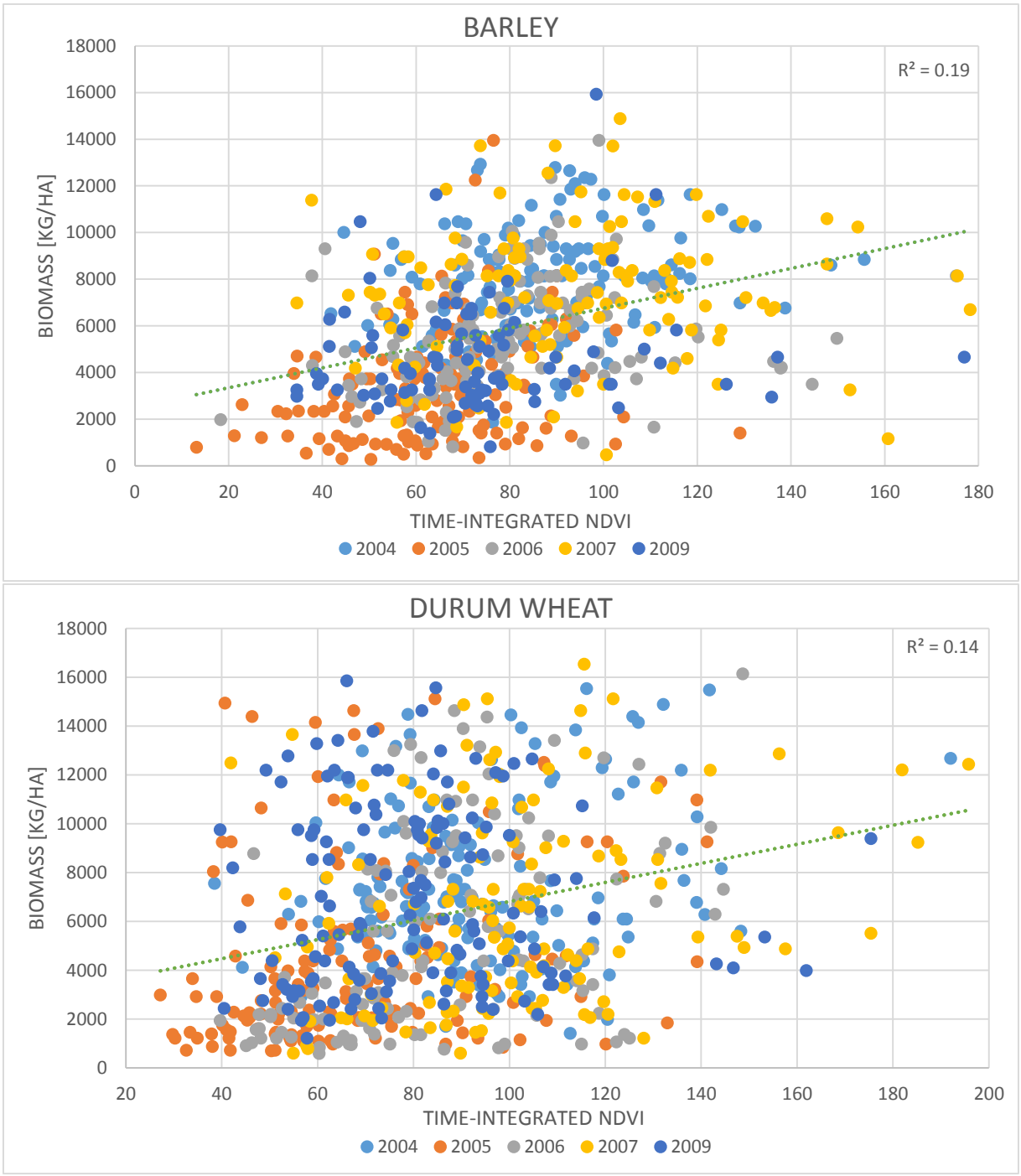

Figure 2.14. Scatterplots and weighted linear models relating barley and durum wheat biomass to Time Integrated NDVI (n=695 for durum wheat, n=641 for barley)

2.5. AquaCrop input files preparation

From the prepared datasets for weather, soil, crop, simulation and RS derived canopy cover, AquaCrop input files are created for each selected sample segment midpoint, in accordance with AquaCrop's specifications as published in the Reference Manuals. This is done with R software. In total 1336 project files and 6615 weather files are created for the simulation runs. In addition one file is created for each crop, containing the RS derived canopy cover and biomass for each selected sample segment midpoint over the respective season. This is done using Microsoft Excel software and R software. The crop files used in the simulation are acquired from FAO, and are initially utilized without any modification.

3. METHOD

3.1. AquaCrop simulations setup

AquaCrop is run in growing degree days (GDD) mode for this research. This approach assures that temperature effects on crop phenology and development are accounted for (FAO, 2012). AquaCrop utilizes a modified procedure based on McMaster and Wilhelm (1997) to calculate GDD. To improve the effect of cold stress on plant processes, minimum temperatures below a plant's base temperature are also considered. In addition to a base temperature, below which the crop is not developing, AquaCrop also utilizes an upper temperature, above which the crop development ceases to increase with temperature. AquaCrop calculates GDD for each day as given in equation (6).

$$GDD = T^*_{avg} - T_{base} \qquad \text{where} \qquad T^*_{avg} = \left(\frac{T^*_{\max} - T_{\min}}{2} \right) \tag{6}$$

With: GDD the growing degree days
T^*_{avg} the adjusted daily average temperature
T_{base} the crop's base temperature
T_{upper} the crop's upper temperature
T_{min} the daily minimum temperature
T^*_{max} the adjusted daily maximum temperature
if the daily maximum temperature > T_{upper} then $T^*_{max} = T_{upper}$
if the daily maximum temperature < T_{base} then $T^*_{max} = T_{base}$

In this method only T^*_{max} is limited by T_{base} and T_{upper} while the effect of daily minimum temperatures below a plant's base temperature is accounted for in the GDD calculation.

As briefly mentioned in chapter 1, AquaCrop uses stress coefficients which adjust target parameters to account for water, temperature and soil stresses on crop development. Some elaboration on this concept is necessary to understand the simulation setup. Figure 3.1 displays the concept of stress factors as used within AquaCrop.

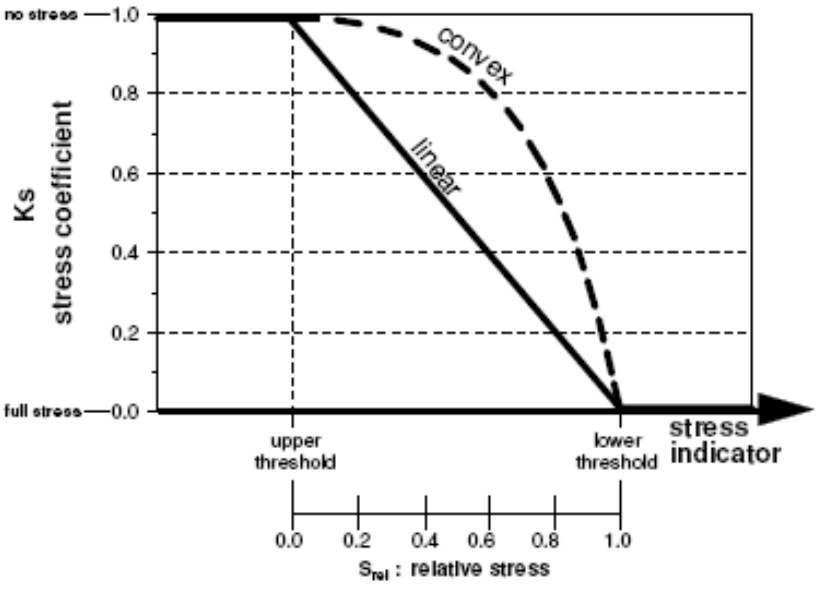

Figure 3.1. The stress coefficient Ks as used in AquaCrop (*FAO,* 2012)

The adjustment of model target parameters by a generic stress coefficient Ks is determined by the thresholds and the shape. The latter sets the sensitivity of the model target parameter while the former defines the range of a stress factor (i.e. soil water content, air temperature, soil salinity, soil fertility) over which the stress coefficient is of influence. Table 3.1 summarizes the stress coefficients used in AquaCrop and their respective model target parameters.

Table 3.1. Summary of stress coefficients used in AquaCrop (Adapted from AquaCrop Reference Manual)

Soil water stress coefficients	**Impact**	**Target model parameter**
$Ks_{exp,w}$ for canopy expansion	Reduces canopy expansion and may have a positive effect on Harvest Index	Crop Growth Coefficient (CGC) and Harvest Index (HI)
Ks_{sto} for stomatal closure	Reduces crop transpiration and root zone expansion and may have a negative effect on Harvest Index	Transpiration (Tr) and Harvest Index (HI)
Ks_{sen} for canopy senescence	Reduces green canopy cover and thus affects crop transpiration	Canopy Cover (CC)
$Ks_{pol,w}$ for pollination	Affects flowering and may have a negative effect on Harvest Index	Harvest Index (HI)
Ks_{aer} for water logging	Reduces crop transpiration	Transpiration (Tr)
Air temperature stress coefficient	**Impact**	**Target model parameter**
Ks_{b} cold stress for biomass production	Reduces biomass production	Normalized Water Productivity (WP*)
$Ks_{pol,c}$ cold stress coefficient for pollination	Affects flowering and may have a negative impact on Harvest Index	Harvest Index (HI)
$Ks_{pol,h}$ heat stress coefficient for pollination	Affects flowering and may have a negative impact on Harvest Index	Harvest Index (HI)
Soil fertility stress coefficient	**Impact**	**Target model parameter**
Ks_{cc} for maximum canopy cover	Reduces canopy cover	Canopy Cover (CC_x)
$Ks_{exp,f}$ for canopy expansion	Reduces canopy expansion	Crop Growth Coefficient (CGC)
Ks_{WP} for water productivity	Reduces biomass production	Normalized Water Productivity (WP*)
$f_{CDecline}$ Decline coefficient of canopy cover	Decline of canopy cover once maximum canopy cover is reached	Canopy Cover (CC_x)
Soil salinity stress coefficient	**Impact**	**Target model parameter**
Ks_{salt}	Reduces biomass production	Transpiration (Tr)
Ks_{cc} for maximum canopy cover	Reduces canopy cover	Canopy Cover (CC_x)
$Ks_{exp,f}$ for canopy expansion	Reduces canopy expansion	Crop Growth Coefficient (CGC)
$Ks_{sto,salt}$ for stomatal closure	Reduces crop transpiration	Water stress coefficient for stomatal closure (Ks_{sto})
$f_{CDecline}$ Decline coefficient of canopy cover	Decline of canopy cover once maximum canopy cover is reached	Canopy Cover (CC_x)

AquaCrop simulations are run for the following four instances:

- **Baseline simulation model.** In this case the standard AquaCrop software is used to process the created project files for 641 barley and 695 durum wheat sample midpoints.
- **Forced biomass simulation model**. In this case, biomass simulated by AquaCrop is replaced after each simulation time step (1 day) by biomass derived from NDVI, using the BIOMASS-TINDVI linear regression models developed in 2.4.3.
- **Forced canopy cover simulation model (a)**. In this case, canopy cover simulated by AquaCrop is replaced after each simulation time step (1 day) by canopy cover derived from NDVI, using Gutman and Ignatov's (1998) dense vegetation mosaic pixel model.
- **Forced canopy cover simulation model (b)**. In this case, canopy cover simulated by AquaCrop is replaced after each simulation time step (1 day) by canopy cover derived from NDVI, using Baret *et al.*'s (1995) gap fraction model.

For the baseline simulation run, FAO's standard crop files for wheat and barley are used with parameters as specified in table 2.3. For the forced simulation runs however, the standard crop files are adjusted in order to eliminate or minimize stress coefficients used in AquaCrop, which account for soil-water and air temperature stresses on crop development. The underlying assumption is that the effect of these stresses is already incorporated in the remotely sensed crop parameters CC or biomass, and therefore no additional adjustments for stresses should be required during forced simulation runs. It remains subject of future research to establish whether the impacts of all stress factors are reflected in NDVI or not. Table 3.2 summarizes the adjusted crop parameters modified for the forced simulation runs.

Table 3.2. Crop parameters as used in forced simulation runs.

Conservative parameter description	Stress Coefficient	Wheat	Barley
Stresses (Soil-water)			
Upper and lower thresholds of soil water depletion for canopy expansion and shape of curve	$Ks_{exp,w}$	0.50/0.80/6.0	0.50/0.80/6.0
Coefficient for positive impact of restricted vegetative growth during yield formation on HI (%)	f_{HI}	0	0
Upper threshold of soil-water depletion for stomatal closure and shape of the stress curve	Ks_{sto}	0.90/6.0	0.90/6.0
Coefficient describing negative impact of stomatal closure during yield formation on HI (%)	f_{HI}	-9.0	-9.0
Upper threshold of soil-water depletion for early senescence and shape of the stress curve	Ks_{sen}	0.98/6.0	0.98/6.0
Upper threshold of soil-water depletion for failure of pollination	$Ks_{pol,w}$	0.98	0.98
Possible increase of HI resulting from water stress before flowering (%)	$Ks_{pol,w}$	0	0
Anaerobiotic point (for effect of waterlogging on transpiration) (Vol %)	Ks_{aer}	-9.0*	-9.0
Stresses (Air Temperature)			
Minimum growing degrees required for full biomass production (°C-days)		-9.0	-9.0

* -9.0 indicates that the parameter is not applicable or not considered. Soil salinity and fertility stresses are not considered in any of the simulation runs.

To run all project files, AquaCrop is used in a batch mode specified as AquaCrop Plugin. The baseline simulation run uses AquaCrop V4.0 and AquaCrop Plugin V4.0, while the forced mode simulations use an adjusted version of AquaCrop and AquaCrop Plugin, in combination with an evaluator module. The adjusted versions of AquaCrop and AquaCrop Plugin have been specifically developed and released for use in this research by Professor D. Raes of the University of Leuven, who is part of the FAO's specialist team that developed AquaCrop. The evaluator module, which feeds the RS-derived CC and biomass into AquaCrop at each simulation time step, is built by Willem Nieuwenhuis, Software Developer at the Natural Resources Department of ITC.

The way forcing works in the setup of this research can best be described as follows. After each simulation step, the adjusted version of AquaCrop records the simulated values of CC and biomass in an exchange file and halts simulation. The evaluator module is allowed to read the exchange file and to overwrite the values of CC and biomass. Once the evaluator has released the exchange file, AquaCrop resumes the simulation. It reads the updated values of CC and biomass and continues its internal calculations for the next simulation step based on the replaced values. The procedure is repeated after each simulation step until simulation end.

The evaluator module allows replacement of simulated by RS-derived values for CC or biomass is performed at each simulation step between start of CGP and end of CGP. The RS derived values for CC or biomass are read from an adequately formatted data-file. The simulation start and end date as well as the start of CGP and end of CGP dates are sample specific and remain the same for each simulation caser. AquaCrop does not consider the end of CGP date, but uses the phenology parameters as specified in the crop files (see table 2.3) to determine the different growth stages during the simulation runs.

3.2. Model validation statistics

Once model simulations have been run, the simulated yields needs to be compared to the observed yields to provide a measure of the model's performance. For this purpose the correlation and regression analysis (Moore et al. 2009) are used on untransformed field measurement (validation) data. In general, the Pearson correlation coefficient r serves as an indicator of the strength and direction of a linear relationship between two variables and is calculated by dividing the covariance of the two variables by the product of their standard deviations, as becomes apparent in its equation (7) shown below.

$$r = \frac{\sum_{i=1}^{n}(x_i - \bar{x}) \cdot (y_i - \bar{y})}{\sqrt{\sum_{i=1}^{n}(x_i - \bar{x})^2 \cdot \sum_{i=1}^{n}(y_i - \bar{y})^2}} \qquad (7)$$

The Pearson correlation coefficient r varies between +1 (for a perfect positive linear relationship) and -1 (in case of a perfect negative linear relationship). Values between -1 and +1 are an indication of the degree of linear relationship between variables. If r equals zero no linear relationship exists between the variables. The linear regression model with a constant, delivering R^2, regression slope and intercept, are additionally used to assess model performance. R^2 determines how much of the linear variation in the observed variable is explained by the variation in the modelled variable. The slope of the linear regression is often considered an indication of model consistency, while the intercept may provide information on model bias (Piñeiro, et al., 2008; Tedeschi, 2006).

Both ordinary and weighted correlation and regression are established for both barley and durum wheat yields and for each simulation case. The weights are calculated using equation (5). Weights are assigned so that more importance is given to sample segments with higher relative crop cover. It is assumed that RS-based data are relatively more accurate when a segment contains relatively more crop. For proper comparison, the baseline simulation (which does not utilize RS data) is treated equally i.e. its output is also evaluated using both ordinary and weighted correlation and regression.

The 1:1 line is the regression line which reflects a perfect model fit. To assess how well the data fits the perfect model, the Nash-Sutcliffe model efficiency coefficient (Nash & Sutcliffe, 1970) is utilized. The Nash-Sutcliffe model efficiency coefficient (NSE) is given by equation (8).

$$NSE = 1 - \frac{\sum_{i=1}^{n}(X_{obs,i} - X_{model,i})^2}{\sum_{i=1}^{n}(X_{obs,i} - \overline{X_{obs}})^2} \qquad (8)$$

Here X_{obs} is the measured or observed value and X_{model} is the modelled value of each sample point. Nash-Sutcliffe efficiencies take values from -∞ to 1. Values below zero indicate unacceptable model performance, while values between 0 and 1 indicate acceptable levels of performance. The model is more accurate as NSE is closer to 1 (Moriasi et al., 2007). A weighted form of NSE exists (Hundecha & Bárdossy, 2004) and is also utilized. Based on Moriasi *et al.* (2007), Chaube *et al.* (2011) devised a performance rating for NSE, which is summarized in table 3.3.

Table 3.3. Performance rating for NSE (Source: Chaube *et al.* 2011)

Performance rating	**NSE**
Very good	0.75- 1.00
Good	0.65- 0.75
Satisfactory	0.5- 0.65
Unsatisfactory	≤ 0.50

To assess model performance the different values of r, R^2 and NSE will be compared across the simulation cases. To quantitatively test the null hypothesis, the correlation coefficients of model output are compared using a procedure developed by R. A. Fisher (1921). In this three-step procedure, the two correlation coefficients are first transformed using equation (9).

$$r' = (0.5)\log_e\left|\frac{1+r}{1-r}\right| \tag{9}$$

In the second step, the test statistic is computed applying equation (10).

$$z = \frac{r_1' - r_2'}{\sqrt{\frac{1}{n_1 - 3} + \frac{1}{n_2 - 3}}} \tag{10}$$

Next the p-value for the derived z is obtained. If the p-value is less than 0.025 (in case of a two-tail test with 95% confidence) r_1 is considered significantly stronger than r_2.

4. RESULTS

4.1. Simulation results

Figure 4.1 illustrates for one actual sample segment midpoint, CC development over the crop growth period for a baseline and a forced-CC simulation run. NDVI is also plotted in the same figure. For the illustrated case a Gutman and Ignatov CC-derivation was applied. This effectively performs a linear transformation on NDVI and consequently, the forced CC simulation closely follows the NDVI pattern.

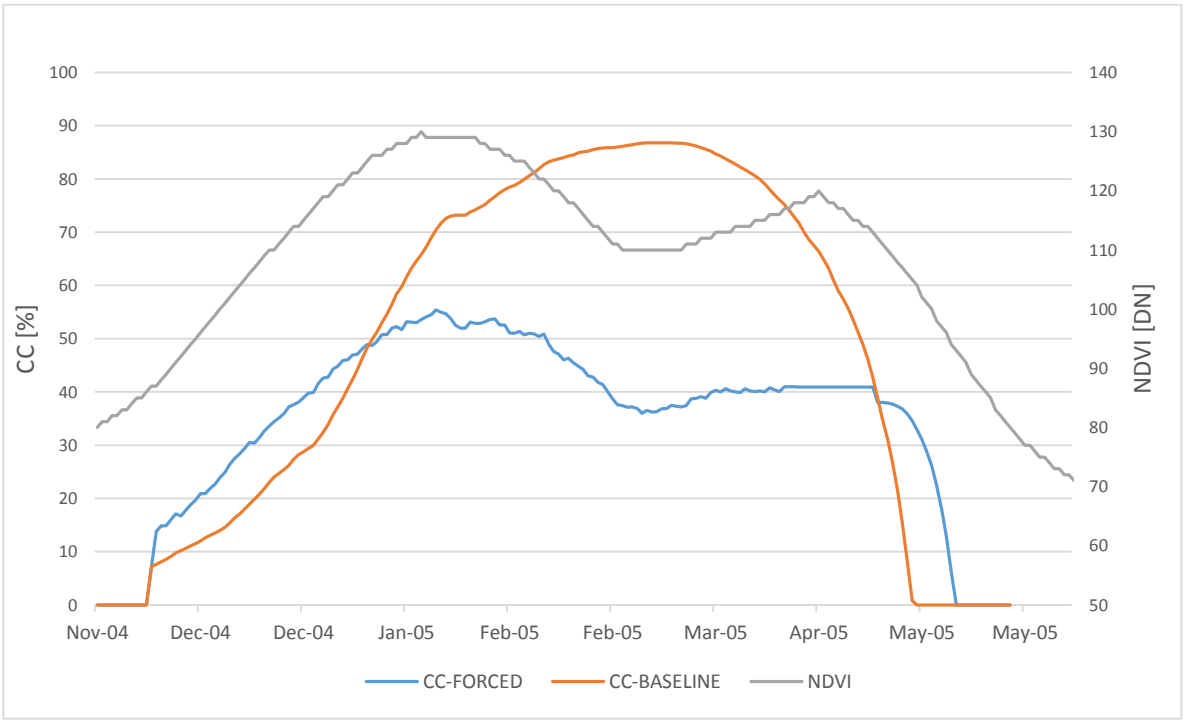

Figure 4.1. CC development in baseline and forced simulation case together with NDVI for the same sample.

Figures 4.2 to 4.5 display the scatterplots with the weighted linear regression line and the 1:1 line for each simulation case, as well as the residual plots. The latter are created to visually assess if the residuals of the regression are independent and identically distributed. This is necessary to determine whether linear regression analysis involving the validation data will still hold or at least be informative for model evaluation. Figures 4.2, 4.4 and 4.5 reasonably confirm independence and identical distribution of the residuals, hence the use of linear regression analysis is justified. Figure 4.3 indicates some dependency in the case of barley, hence the use of linear regression analysis may not be justified here. Finally, table 4.1 summarizes the results of all statistical tests performed for all simulation cases.

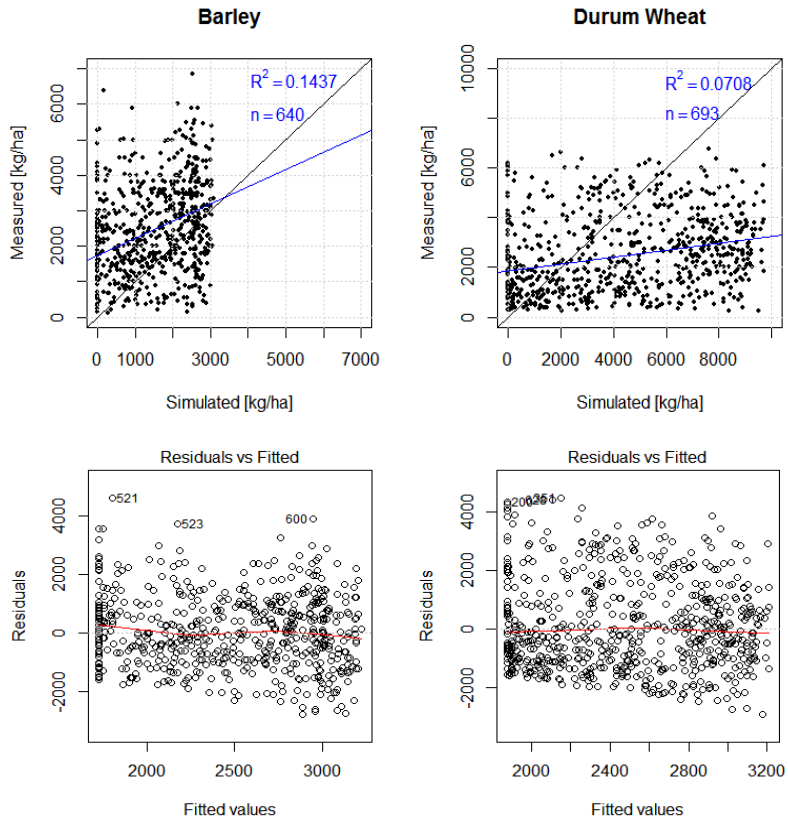

Figure 4.2. Scatterplots with weighted linear regression lines and residual plots for AquaCrop's baseline simulation run

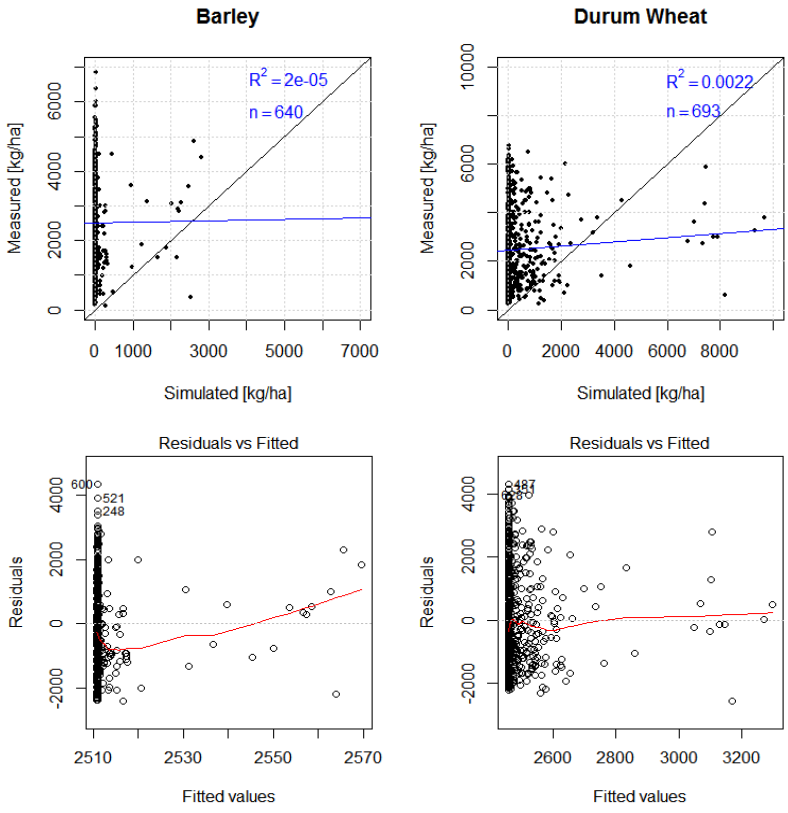

Figure 4.3. Scatterplots with weighted linear regression lines and residual plots for AquaCrop's simulation run with forced RS-derived biomass utilizing the TINDVI-Biomass relationship

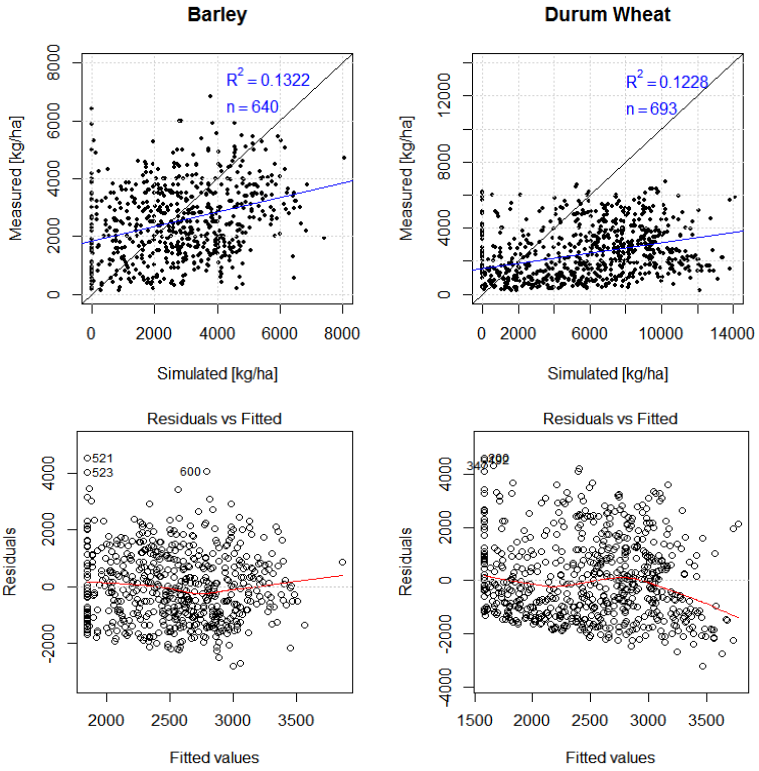

Figure 4.4. Scatterplots with weighted linear regression lines and residual plots for AquaCrop's simulation run with forced RS-derived CC utilizing Gutman and Ignatov's model

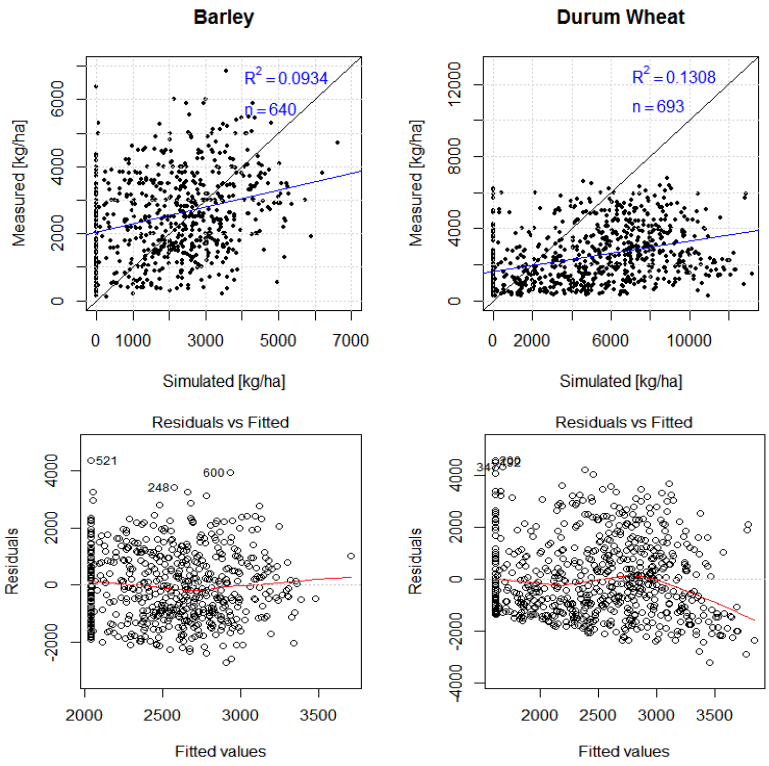

Figure 4.5. Scatterplots with weighted linear regression lines and residual plots for AquaCrop's simulation run with forced RS-derived CC utilizing Baret *et al.*'s model

Table 4.1. Summary of model evaluation results for all simulation cases

		*AquaCrop_STD	**AquaCrop_BM	***AquaCrop_GI	****AquaCrop_BA
BARLEY	r	0.38	0	0.36	0.31
	R^2	0.14	0	0.13	0.09
	Intercept	1725(s)	2511(s)	1850(s)	2039(s)
	Slope	0.49(s)	0.02 (n.s.)	0.25(s)	0.25(s)
	NSE	-0.54	-143.22	-1.06	-1
DURUM WHEAT	r	0.27	0.05	0.35	0.36
	R^2	0.07	0.002	0.12	0.13
	Intercept	1876(s)	2459(s)	1580(s)	1615(s)
	Slope	0.14(s)	0.09(n.s.)	0.16(s)	0.17(s)
	NSE	-3.33	-9.93	-8.25	-6.17

s indicates a significant p-value ($p < 0.05$)
n.s. indicates a non-significant p-value ($p < 0.05$)
*AquaCrop_STD refers to the baseline simulation,
**AquaCrop_BM refers to the simulation with RS-forced biomass
***AquaCrop_GI refers to the simulation with RS-forced CC utilizing Gutman & Ignatov's model
****AquaCrop_BA refers to the simulation with RS-forced CC utilizing Baret et al's model

From the results it becomes apparent that none of the simulation models performs satisfactory. NSE values are all less than zero with the worst results attributed to the forced biomass simulation case. Only in the case of durum wheat, both RS-forced CC simulations indicate a slightly improved model performance.

4.2. Hypothesis test

To quantitatively test the null hypothesis, the correlation coefficients of model output are compared using a procedure developed by R. A. Fisher (1921) which is explained in section 3.2. Table 4.2 summarizes the calculation results.

Table 4.2. Summary of Fisher test for the comparison of correlation coefficients

		*AquaCrop_STD	**AquaCrop_GI
BARLEY	r	0.38	0.36
	n	640	640
	z	0.41	
	p-value	0.34	
D-WHEAT	r	0.27	0.36
	n	693	693
	z	-1.86	
	p-value	0.03	

*AquaCrop_STD refers to the baseline simulation
**AquaCrop_GI refers to the simulation with RS-forced CC utilizing Gutman & Ignatov's model

With one-tailed p-values at 0.34 and 0.03 we cannot reject the null hypothesis, hence the accuracy of actual yield estimations in the AquaCrop model that utilizes RS data is not significantly better than the accuracy of yield estimations derived from the AquaCrop model without the use of RS data.

5. DISCUSSION

5.1. Introduction

This research explored forcing of RS-derived canopy cover and biomass into the AquaCrop crop growth model for actual field conditions at a regional level. The use of RS data in AquaCrop is expected to lead to more accurate and more robust actual yield estimations because it contains actual empirical information of the crop's growth state throughout the crop's lifecycle. However, the results of the research are not in agreement with the a priori expectations. In the discussion presented here, different aspects of the research are critically examined, with the objective of identifying and disclosing potential weaknesses, with discussions on possible ways forward.

5.2. Exploring the simulation results

From the results of the simulation runs (i.e. figures 4.2-4.5), it can be observed that only in the case of forced biomass a significant but negative impact on model performance occurs. For the forced CC simulations however, there seems to be no clear effect on model performance. A general increase in simulated yield values is apparent, however this may be due to the fact that stress factors in the RS-forced simulation runs have been minimized or completely disregarded. A more detailed exploration of the simulation runs may provide insight. For that purpose the results of the AquaCrop_STD case are plotted against the results of the AquaCrop_GI case. Figure 5.1 shows the scatter diagrams for both barley and durum wheat. A considerable correlation (r=0.45 and 0.67 for barley and durum wheat respectively) is apparent between the AquaCrop_STD and the AquaCrop_GI simulations for durum wheat and to a lesser extent for barley. The forcing of RS-based CC does affect the estimated yields, however to different extent for barley and durum wheat.

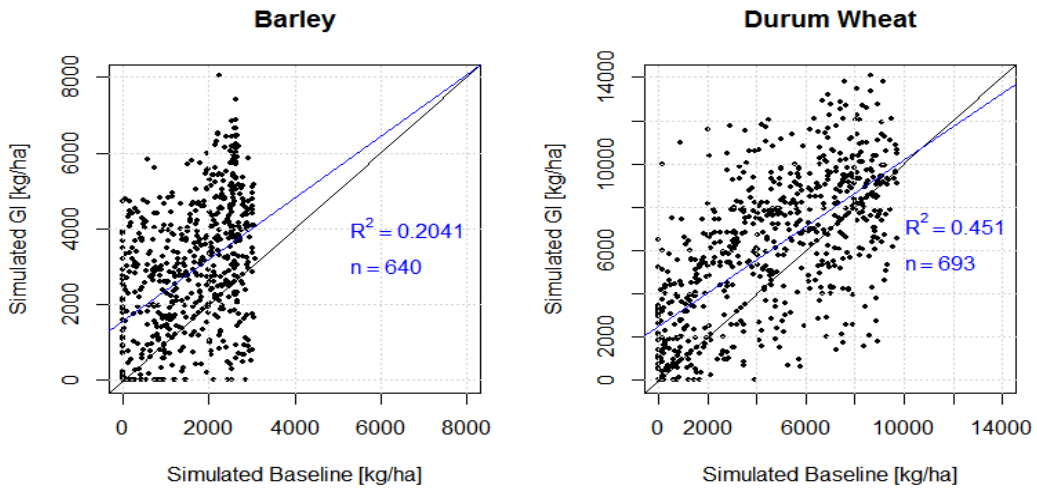

Figure 5.1. Scatterplots with linear regression lines for AquaCrop's baseline simulation against AquaCrop's forced RS-derived CC utilizing Gutman and Ignatov's model

Next, a number of simulation results from the baseline simulation and RS-forced CC simulations derived by Gutman and Ignatov's model are inspected. Considering that each simulation case can either result in an underestimation (U), correct estimation (OK) or overestimation (O) of yield, several combinations have been explored. Figure 5.2 shows the CC development compared to NDVI for some selected samples and cases.

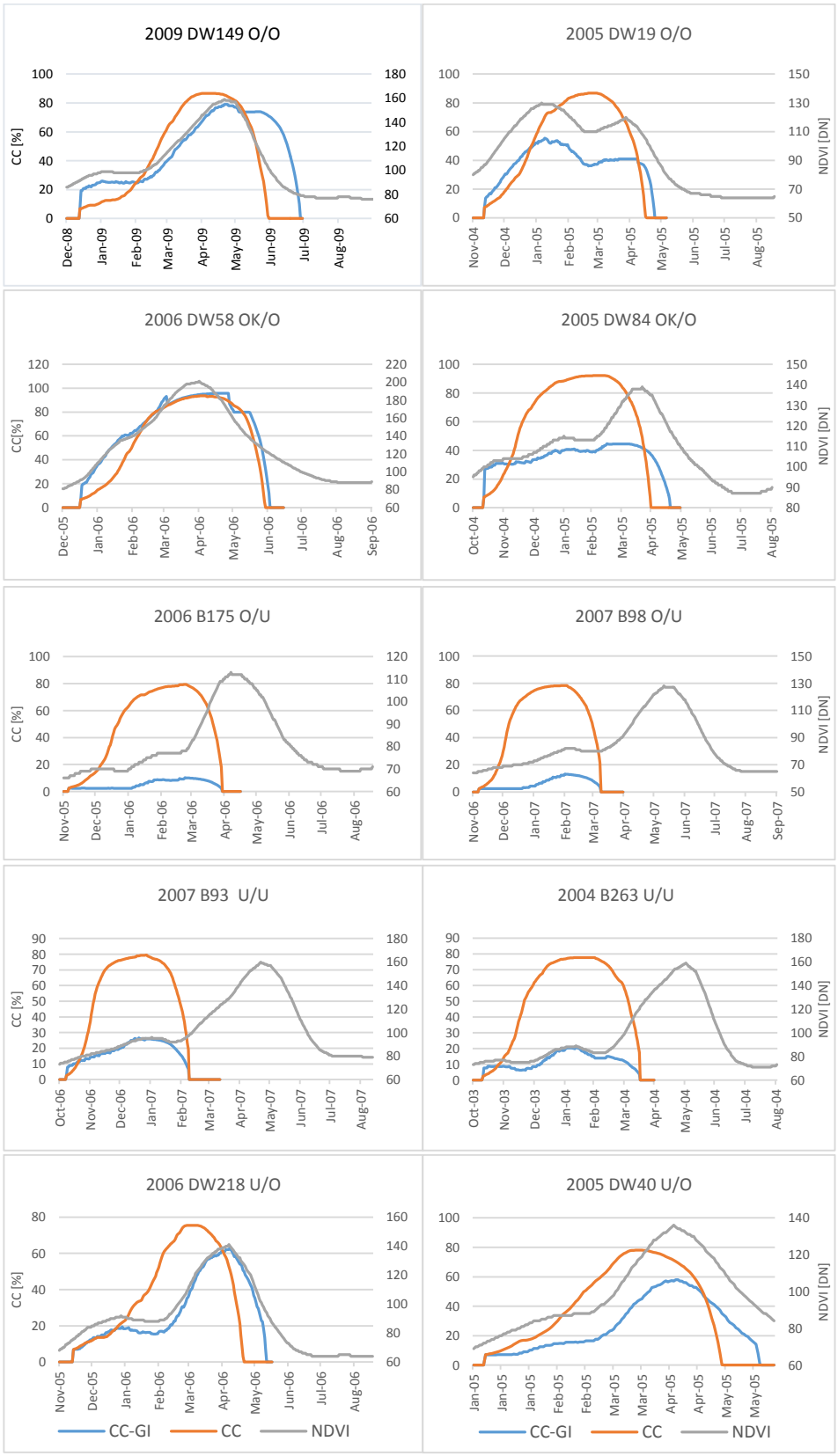

Figure 5.2. CC-development throughout growing season compared to NDVI for some sample midpoints. Graph titles indicate year, crop (B=Barley, DW= Durum Wheat), sample number and explored case (baseline/forced with U= underestimation, O = overestimation, OK = correct estimation). CC indicates baseline, CC-GI indicates RS-forced simulation canopy cover.

Drawing solid conclusions from the graphs in figure 5.2 is challenging. It is however obvious that the crop phenology in simulations often disagrees with the crop phenology as suggested by the NDVI pattern. Reference is made to figures 2.8 and 2.10 that respectively show crop phenology indicators in relationship to NDVI and the expected agreement of NDVI and CC-development in AquaCrop simulations, irrespective of the use of forcing. To further investigate this disagreement, the length of the crop growing period (CGP) as derived from NDVI in chapter 2, is compared to the length of the growing cycle in AquaCrop for each simulation run. The latter is expected to be similar for all simulation cases since the growing cycle is determined by AquaCrop based on GDD, which is similar in all cases. For this comparison, the simulation output for the AquaCrop_GI case has been utilized. Figure 5.3 summarizes the results.

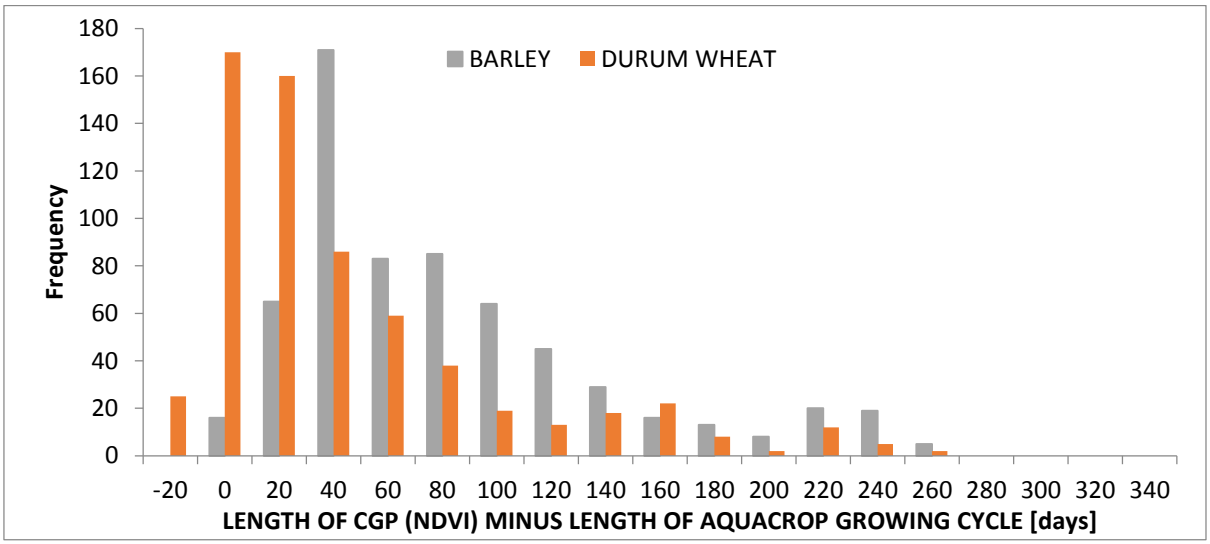

Figure 5.3. Histogram of the difference between crop phenology derived from NDVI (CGP) compared to crop phenology derived by AquaCrop for (growing cycle) for all simulated sample segments (693 durum wheat and 640 barley)

Following figure 5.3, the simulations in AquaCrop are in considerable disagreement with reality (under the assumption that NDVI represents reality) with regards to crop phenology. As a consequence, AquaCrop's estimated yields for this research have little to no relationship with the actual development of the crop. This observation identifies a major issue during simulations performed in section 3.3 and section 3.4 and feeds the forthcoming discussion.

For this research AquaCrop is run in GDD mode. The different phenology phases in crop development are expressed in number of GDD's. AquaCrop calculates the GDD's based on temperature input data and uses the crop's parameters for the base and upper temperature as given in the crop file to determine the crop's phenology. In most cases AquaCrop terminates crop growth before the crop actually ceases to grow. For barley sample segments, figure 5.3 shows that the deviation is generally larger than for durum wheat. This may be due to its lower time to maturity parameter setting in AquaCrop (1296 vs 2400 GDD's for barley and durum wheat respectively). The actual error in yield estimations this leads to, needs to be established through a more detailed analysis. Figure 5.1 however indicates the appearance of systematic underestimation for the RS-forced simulation case when the crop's growing period is terminated early. Because AquaCrop simulations seem to systematically terminate crop growth early, there is suspicion that the 0 °C base temperatures for both crops is too low. Crop temperature settings are considered to be made in a conservative manner (FAO, 2012); they should hold for the same crop irrespective of location. This finding however indicates that calibration of also the conservative crop parameters to achieve accurate and reliable estimations is required.

To address the discrepancy between crop phenology in AquaCrop simulations and reality, two approaches can be considered. The first is to (iteratively) adjust the crop base and upper temperature input parameters. The second option is to defer from running simulations in GDD mode and to run simulations in normal time. The different crop phenology stages are then defined in calendar days and may either be derived from existing data for the crop and region under evaluation or from remote sensing data. Multi-temporal NDVI for example can aid in identifying the occurrence of different phases in phenology. Extending on the approach by Reed *et al.* (1994), additional metrics can be derived from NDVI for this purpose (Hill & Donald, 2003; Zhao et al., 2012).

5.3. AquaCrop model sensitivity

AquaCrop models crop growth throughout the crop's lifecycle. For this purpose the crop and its environment are characterized by quantitative metrics on the basis of which AquaCrop is able to calculate the crop development and ultimately estimate yield. Figure 5.4 shows a simplified overview of the simulations in AquaCrop. In general, yield estimations from AquaCrop are subject to errors in input data for crop and environment as well as generalizations within the model itself. The latter will not be considered here for two reasons. Firstly, the general results with AquaCrop around the world so far, despite its main use on local scale, give no immediate reason to doubt the model itself. Secondly, the user has no direct options to modify adopted mechanisms of the model.

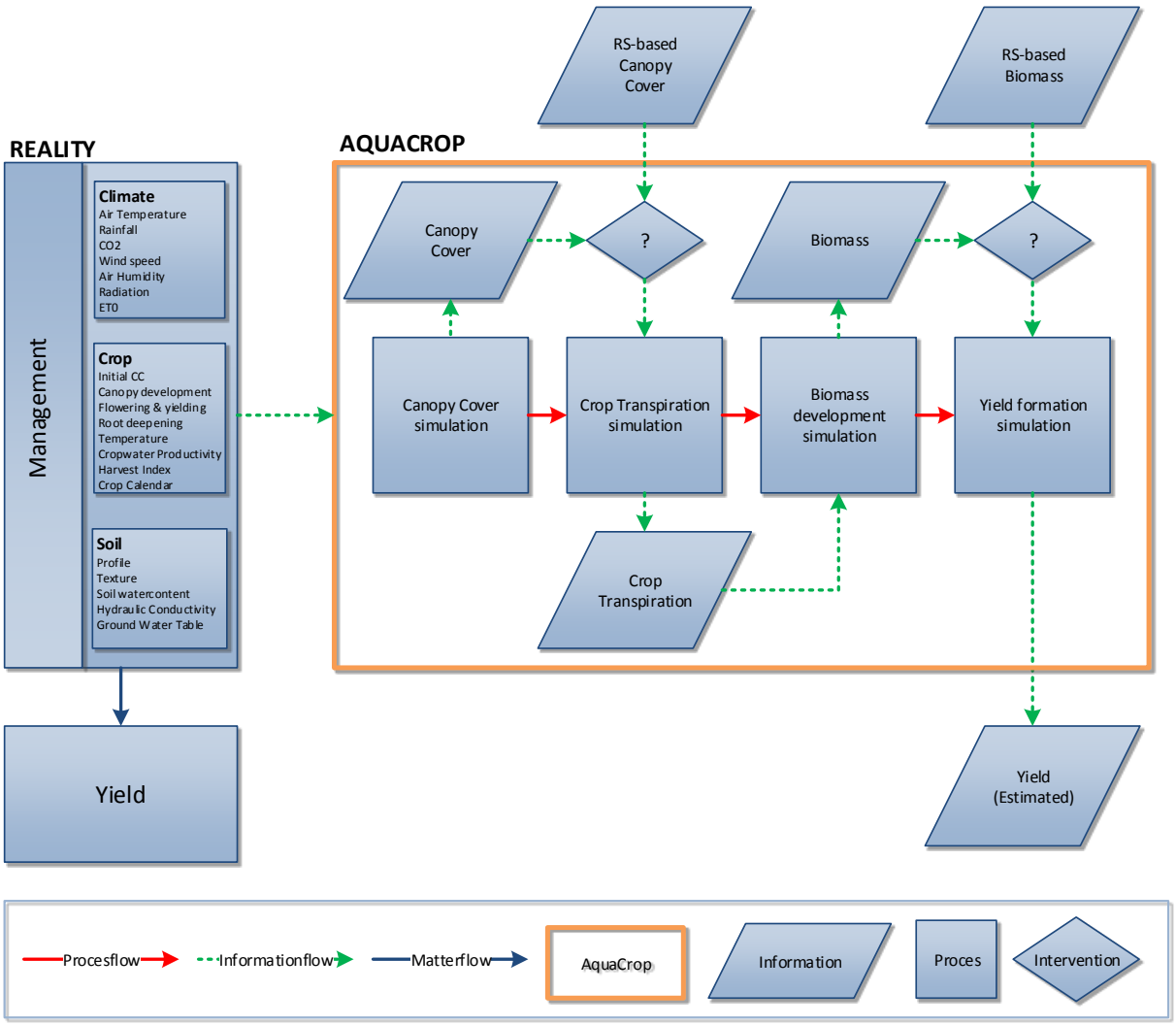

Figure 5.4. Simplified overview of simulations in AquaCrop

The information provided to AquaCrop originates from various sources and has been processed in different ways in preparation (see chapter 2). The data acquisition and data processing, including applied assumptions and simplifications, are all sources of inaccuracies that ultimately influence the yield estimation. This applies to information regarding climate, soil and crop as well as to RS-derived data regarding crop phenology, CC and biomass. Understanding the model's sensitivity to variance in input data is not only required when trying to understand errors in yield estimation, but also in prioritizing efforts to improve model performance. AquaCrop's documentation and literature (Geerts et al., 2009; Salemi et al., 2011) provide some direction in this area.

Most studies involving the use of AquaCrop, have focussed on yield estimation at local level for research station conditions, for which the information requirements to adequately characterize crop and environment can be met confidently. Challenges to meet AquaCrop's information requirements arise when AquaCrop is used for regional monitoring of production. The use of RS-data to characterize crop and environment is inevitable at this scale, at least for some parameters. Determining the required spatial and temporal resolutions as well as appropriate data processing techniques (e.g. for spatial or temporal data interpolation) is subject to solid understanding of the model sensitivity. Recently a global sensitivity analysis for AquaCrop has been conducted (Vanuytrecht et al., 2014), identifying influential and non-influential model parameters and providing guiding principles to AquaCrop users.

5.4. Representativeness of NDVI time series

For this research it was assumed that CGP, canopy cover and biomass derived from NDVI time series provide a good measure of the crop's actual state. However, the NDVI time series for each pixel is not solely related to the crop under investigation, due to several factors. First there a discrepancy between sample segment size (700x700m) and the utilized NDVI pixel size (1x1km). Secondly it is possible to have one sample segment fall within multiple adjacent NDVI pixels. Thirdly, the sample segments are heterogeneous whereby barley and durum wheat occupy only a small fraction in most cases (see figure 2.2). These factors are sources of inaccuracy. Not only could they lead to inaccuracies in biomass or canopy cover proxies derived from the NDVI time series, but they may also explain the observed deviations between NDVI-derived CGP and AquaCrop's growing cycle. To address these inaccuracies, utilization of higher resolution NDVI time series, like MODIS (16-days 250x250m pixel size) or PROBA-V (10 days 1/3 x 1/3 km pixel size) may be considered.

5.5. Remote sensing proxies for canopy cover and biomass

For this research, remote sensing proxies for canopy cover and biomass have been derived from NDVI. Although this research has not established to which extent NDVI-derived proxies satisfy the requirements for accurate yield estimations, it may be useful to explore alternative options, especially if the RS-forced simulations are extended to other regions. Accurate optical RS data may for instance be difficult to acquire over the cropping season in regions with substantial cloud cover. In those cases the synthesis with synthetic aperture radar (SAR) may be considered (Bach et al., 2012).

Jiang *et al.* (2006) introduced a scaled difference vegetation index (SDVI), also based on red and near infrared reflectances and showed that SDVI is a better proxy for canopy cover, especially for heterogeneous surfaces, than the models proposed by Gutman and Ignatov (1998) and Baret *et al.* (1995). Gitelson (2004) proposed the derivation of canopy cover utilizing a Wide Dynamic Range Vegetation Index (WDRVI). In another study (Gitelson, 2013) he compared the use of WDRVI for canopy cover retrieval to six other vegetation indices for maize and soybean.

Additionally the work of Jiapaer *et al.* (2011) provides valuable information with regards to the use of alternatives to NDVI when deriving canopy cover. They compared the use of six kinds of remote sensing inversion models (NDVI regression, a spectral mixture analysis, pixel dichotomy and three 3-band maximal gradient difference models). Bao et al. (2008) correlated biomass of wheat to vegetation indices derived from TM data and showed that different vegetation indices were optimal for different growth stages. Combining different vegetation indices may lead to improved biomass proxies. Alternatively the utilization of SAR (Dente et al., 2008; Moran et al., 2012) for crop biomass estimations throughout the growth season could be considered. Another interesting approach is the derivation of crop properties by inverse radiative transfer modelling (Ha, 2013; Jacquemoud et al., 1995; Verhoef & Bach, 2007).

5.6. Concluding considerations

Crop growth simulation modelling for food security is in itself an extensive area of research. An endless amount of aspects must be considered. The purpose of this thesis is not to be complete, but only to indicate some main issues for further considerations. Two additional aspects related to this research worth mentioning are the following. First, the use of AquaCrop at a regional level, requires an extensive amount of data processing, both in preparation to the simulations as well as in processing simulation output. AquaCrop has not been built for this type of application. Once proven of use, it would be worthwhile to consider embedding AquaCrop into a data processing environment (or application), which accommodates the use of AquaCrop at the spatial scales required for food security studies. Some work has been done in that area (Lorite et al., 2013) however the products developed (AquaData & AquaGIS) are not yet available for use or evaluation. Another interesting aspect is related to the use of RS-derived crop parameters i.e. for crop phenology. Instead of determining crop phenology beforehand (whether or not from RS-data) and fixing this into AquaCrop, re-parameterization (Maas, 1988) of AquaCrop during simulation runs could be considered based on actual remotely sensed observations of crop phenology. Combining calibration with forcing however poses new challenges (Clevers et al., 2002; Launay & Guerif, 2005).

6. CONCLUSIONS AND RECOMMENDATIONS

6.1. Conclusions

The use of Remote Sensing data in a crop growth model to estimate actual crop yields has been evaluated. NDVI time series derived canopy cover and biomass has been forced into AquaCrop for barley and durum wheat in Spain for five growing seasons within the period of 2004 to 2009. The following conclusions can be drawn from the research.

- Forcing NDVI-derived canopy cover or biomass did not improve AquaCrop's performance as compared to the use of AquaCrop without forcing. The simulation runs where NDVI-based biomass was forced into AquaCrop show no correlation between observed and modelled output, while simulation runs where NDVI-based canopy cover was forced into AquaCrop show no significant improvement of model performance.
- Many sources of inaccuracy may exist in the applied method, varying from inaccuracies in data measurements, model parameterization, data-processing, and applied assumptions and simplifications. Determining the required spatial and temporal resolutions for data as well as appropriate data processing techniques is subject to solid understanding of the model sensitivity. In addition, establishing the model's sensitivity to variance in input data is necessary in order to analyze errors in yield estimation and in prioritizing efforts to improve model performance.
- The crop phenology in simulation runs (baseline, forced canopy cover, forced biomass) for the majority of selected samples does not agree with crop phenology derived from NDVI time series. Crop base temperature is suspect of being too low, however other crop parameters may be suspect as well.
- Inaccuracies in biomass or canopy cover proxies and CGP derived from the NDVI time series can result from sample segment heterogeneity. Sample segments are smaller than utilized NDVI pixels. In addition barley and durum wheat occupy only a small fraction in most sample segments. As a result, the NDVI signal may not be very representative of the crop under evaluation.

6.2. Recommendations

Drawing upon the conclusions, the following recommendations for future research can be formulated.

- Firstly, it is recommended to establish AquaCrop's sensitivity to variance in input data, both related to the crop as well as the environment. Determining the model's sensitivity to variance in input data, will aid in estimated yield error analyses and in prioritizing efforts to improve model performance. Guiding principles, resulting from a global AquaCrop sensitivity analysis have recently been published (Vanuytrecht et al., 2014) and can be utilized.
- An additional recommendation following the observed discrepancy between simulated and NDVI-derived crop phenology, is to calibrate AquaCrop for the crops and location under evaluation.
- The final recommendation is to explore higher resolution NDVI time series, both for derivation of CGP as well as biomass and canopy cover. MODIS (16-days 250x250m pixel size) or PROBA-V (10 days 1/3 x 1/3 km pixel size) may be considered. Considering the heterogeneous cover in sample segments, a more representative NDVI signal for the crops may then be retrieved. In addition other vegetation indices, the (complementary) use of SAR or inverse radiative transfer modelling may proof useful.

LIST OF REFERENCES

Abedinpour, M., Sarangi, A., Rajput, T. B. S., Singh, M., Pathak, H., & Ahmad, T. (2012). Performance evaluation of AquaCrop model for maize crop in a semi-arid environment. *Agricultural Water Management, 110*, 55-66. doi: 10.1016/j.agwat.2012.04.001

Abrha, B., Delbecque, N., Raes, D., Tsegay, A., Todorovic, M., Heng, L., Deckers, S. (2012). Sowing strategies for barley (hordeum vulgare l.) based on modelled yield response to water with aquacrop. *Experimental Agriculture, 48*(2), 252-271. doi: 10.1017/s0014479711001190

Albrizio, R., Todorovic, M., Matic, T., & Stellacci, A. M. (2010). Comparing the interactive effects of water and nitrogen on durum wheat and barley grown in a Mediterranean environment. *Field Crops Research, 115*(2), 179-190. doi: 10.1016/j.fcr.2009.11.003

Alexandratos, N., & Bruinsma, J. (2012). *World Agriculture Towards 2030/2050: The 2012 Revision*.

Allen, R. G., Pereira, L. S., Raes, D., & Smith, M. (1998). *Crop evapotranspiration. Guidelines for computing crop water requirements*. Rome: FAO.

Andarzian, B., Bannayan, M., Steduto, P., Mazraeh, H., Barati, M. E., Barati, M. A., & Rahnama, A. (2011). Validation and testing of the AquaCrop model under full and deficit irrigated wheat production in Iran. *Agricultural Water Management, 100*(1), 1-8. doi: 10.1016/j.agwat.2011.08.023

Apaydin, H., Sonmez, F. K., & Yildirim, Y. E. (2004). Spatial interpolation techniques for climate data in the GAP region in Turkey. *Climate Research, 28*(1), 31-40. doi: 10.3354/cr028031

Araya, A., Habtu, S., Hadgu, K. M., Kebede, A., & Dejene, T. (2010). Test of AquaCrop model in simulating biomass and yield of water deficient and irrigated barley (Hordeum vulgare). *Agricultural Water Management, 97*(11), 1838-1846. doi: 10.1016/j.agwat.2010.06.021

Attorre, F., Alfo, M., De Sanctis, M., Francesconi, F., & Bruno, F. (2007). Comparison of interpolation methods for mapping climatic and bioclimatic variables at regional scale. *International Journal of Climatology, 27*(13), 1825-1843. doi: 10.1002/joc.1495

Aparicio N., Villegas D., Casadesús J., Araus J.L., Royo C. Canopy reflectancre indices: A new tool for assessing durum wheat LAI and yield. In: Royo C. (ed.), Nachit M. (ed.), Di Fonzo N. (ed.), Araus J.L. (ed.). Durum wheat improvement in the Mediterranean region: New challenges. Zaragoza: CIHEAM, 2000. p. 117-119 (Options Méditerranéenes: Série A. Séminaires Méditerranéens; n. 40)

Bach, H., Friese, M., Spannraft, K., Migdall, S., Dotzler, S., Hank, T., Ieee. (2012). Integrative use of multitemporal rapideye and terrasar-x data for agricultural monitoring. *2012 Ieee International Geoscience and Remote Sensing Symposium (Igarss)*, 3748-3751.

Bao, Y. S., Gao, W., & Gao, Z. Q. (2008). Estimating winter wheat biomass based on LANDSAT TM and MODIS data. In W. Gao & H. Wang (Eds.), *Remote Sensing and Modeling of Ecosystems for Sustainability V* (Vol. 7083). Bellingham: Spie-Int Soc Optical Engineering.

Baret, F., Clevers, J., & Steven, M. D. (1995). The robustness of canopy gap fraction estimates from red and near-infrared reflectances - a comparison of approaches. *Remote Sensing of Environment, 54*(2), 141-151. doi: 10.1016/0034-4257(95)00136-o

Bennett, N. D., Croke, B. F. W., Guariso, G., Guillaume, J. H. A., Hamilton, S. H., Jakeman, A. J., . . . Andreassian, V. (2013). Characterising performance of environmental models. *Environmental Modelling & Software, 40*(0), 1-20. doi: http://dx.doi.org/10.1016/j.envsoft.2012.09.011

Beurs, K., & Henebry, G. (2010). Spatio-Temporal Statistical Methods for Modelling Land Surface Phenology. In I. L. Hudson & M. R. Keatley (Eds.), *Phenological Research* (pp. 177-208): Springer Netherlands.

Box, G. E. P., & Cox, D. R. (1964). An analysis of transformations. *Journal of the Royal Statistical Society Series B-Statistical Methodology, 26*(2), 211-252.

Brown, J. F., Reed, B. C., Hayes, M. J., Wilhite, D. A., & Hubbard, K. (2002). *A prototype drought monitoring system integrating climate and satellite data.* Paper presented at the Pecora 15/Land satellite Information IV/ISPRS commission I/FIEOS 2002, Denver Colorado.

Calera, A., Gonzalez-Piqueras, J., & Melia, J. (2004). Monitoring barley and corn growth from remote sensing data at field scale. *International Journal of Remote Sensing, 25*(1), 97-109. doi: 10.1080/0143116031000115319

Cantero-Martínez, C., Angas, P., & Lampurlanés, J. (2003). Growth, yield and water productivity of barley (Hordeum vulgare L.) affected by tillage and N fertilization in Mediterranean semiarid, rainfed

conditions of Spain. *Field Crops Research, 84*(3), 341-357. doi: http://dx.doi.org/10.1016/S0378-4290(03)00101-1

Cao, W. J., Hu, J. X., & Yu, X. M. (2009). *A Study on Temperature Interpolation Methods Based on GIS*. New York: Ieee.

Casa, R., Varella, H., Buis, S., Guerif, M., De Solan, B., & Baret, F. (2012). Forcing a wheat crop model with LAI data to access agronomic variables: Evaluation of the impact of model and LAI uncertainties and comparison with an empirical approach. *European Journal of Agronomy, 37*(1), 1-10. doi: 10.1016/j.eja.2011.09.004

Chen, J., Jönsson, P., Tamura, M., Gu, Z., Matsushita, B., & Eklundh, L. (2004). A simple method for reconstructing a high-quality NDVI time-series data set based on the Savitzky–Golay filter. *Remote Sensing of Environment, 91*(3–4), 332-344. doi: http://dx.doi.org/10.1016/j.rse.2004.03.014

Clevers, J., Vonder, O. W., Jongschaap, R. E. E., Desprats, J. F., King, C., Prevot, L., & Bruguier, N. (2002). Using SPOT data for calibrating a wheat growth model under mediterranean conditions. *Agronomie, 22*(6), 687-694. doi: 10.1051/agro:2002038

Curnel, Y.; Oger, R. Agrophenology indicators from remote sensing: state of the art. The International Archives of the Photogrammetry, Remote Sensing and Spatial Information Sciences, tome XXXVI-8/W48, Stresa (IT), p. 31-38, 2006.

Curnel, Y., de Wit, A. J. W., Duveiller, G., & Defourny, P. (2011). Potential performances of remotely sensed LAI assimilation in WOFOST model based on an OSS Experiment. *Agricultural and Forest Meteorology, 151*(12), 1843-1855. doi: http://dx.doi.org/10.1016/j.agrformet.2011.08.002

De Bie, C. A. J. M., & Morsink, K. (2013). Earth Observation-derived yield assessments for index insurance in agriculture: logic of variability sources and reality. In R. Gommes & F. Kayitakire (Eds.), *The challenges of index-based insurance for food security in developing countries* (pp. 276). Luxembourg: European Union.

de Wit, A. J. W., & van Diepen, C. A. (2008). Crop growth modelling and crop yield forecasting using satellite-derived meteorological inputs. *International Journal of Applied Earth Observation and Geoinformation, 10*(4), 414-425. doi: 10.1016/j.jag.2007.10.004

Delécolle, R., Maas, S. J., Guérif, M., & Baret, F. (1992). Remote sensing and crop production models: present trends. *ISPRS Journal of Photogrammetry and Remote Sensing, 47*(2–3), 145-161. doi: http://dx.doi.org/10.1016/0924-2716(92)90030-D

Dente, L., Satalino, G., Mattia, F., & Rinaldi, M. (2008). Assimilation of leaf area index derived from ASAR and MERIS data into CERES-Wheat model to map wheat yield. *Remote Sensing of Environment, 112*(4), 1395-1407. doi: http://dx.doi.org/10.1016/j.rse.2007.05.023

Dinku, T., Chidzambwa, S., Ceccato, P., Connor, S. J., & Ropelewski, C. F. (2008). Validation of high-resolution satellite rainfall products over complex terrain. *International Journal of Remote Sensing, 29*(14), 4097-4110. doi: 10.1080/01431160701772526

Dinku, T., Ruiz, F., Connor, S. J., & Ceccato, P. (2010). Validation and Intercomparison of Satellite Rainfall Estimates over Colombia. *Journal of Applied Meteorology and Climatology, 49*(5), 1004-1014. doi: 10.1175/2009jamc2260.1

Diouf, A., & Lambin, E. F. (2001). Monitoring land-cover changes in semi-arid regions: remote sensing data and field observations in the Ferlo, Senegal. *Journal of Arid Environments, 48*(2), 129-148. doi: 10.1006/jare.2000.0744

Doorenbos, J., & Kassam, A. H. (1979). Yield response to water. *Irrigation and Drainage Paper No. 33. FAO, Rome*.

Doraiswamy, P. C., Hatfield, J. L., Jackson, T. J., Akhmedov, B., Prueger, J., & Stern, A. (2004). Crop condition and yield simulations using Landsat and MODIS. *Remote Sensing of Environment, 92*(4), 548-559. doi: 10.1016/j.rse.2004.05.017

FAO, 2012. *Crop yield response to water* (2012). Rome.

Fisher, R. A. (1921). On the probable error of a coefficient of correlation deduced from a small sample. *Metron, 1*, 3-32. doi: citeulike-article-id:2346712

Geerts, S., Raes, D., Garcia, M., Miranda, R., Cusicanqui, J. A., Taboada, C., . . . Steduto, P. (2009). Simulating Yield Response of Quinoa to Water Availability with AquaCrop. *Agronomy Journal, 101*(3), 499-508. doi: 10.2134/agronj2008.0137s

Gitelson, A. A. (2004). Wide Dynamic Range Vegetation Index for Remote Quantification of Biophysical Characteristics of Vegetation. *Journal of Plant Physiology, 161*(2), 165-173. doi: http://dx.doi.org/10.1078/0176-1617-01176

Gitelson, A. A. (2013). Remote estimation of crop fractional vegetation cover: the use of noise equivalent as an indicator of performance of vegetation indices. *International Journal of Remote Sensing, 34*(17), 6054-6066. doi: 10.1080/01431161.2013.793868

Glenn, E. P., Huete, A. R., Nagler, P. L., & Nelson, S. G. (2008). Relationship between remotely-sensed vegetation indices, canopy attributes and plant physiological processes: What vegetation indices can and cannot tell us about the landscape. *Sensors, 8*(4), 2136-2160. doi: 10.3390/s8042136

Gutman, G., & Ignatov, A. (1998). The derivation of the green vegetation fraction from NOAA/AVHRR data for use in numerical weather prediction models. *International Journal of Remote Sensing, 19*(8), 1533-1543. doi: 10.1080/014311698215333

Ha, N. T. T. (2013). *Earth observation for rice crop monitoring and yield estimation : application of satellite data and physically based models to the Mekong Delta.* (222), University of Twente Faculty of Geo-Information and Earth Observation (ITC), Enschede. Retrieved from http://www.itc.nl/library/papers_2013/phd/nguyenha.pdf

Hansen, J. W., & Jones, J. W. (2000). Scaling-up crop models for climate variability applications. *Agricultural Systems, 65*(1), 43-72. doi: 10.1016/s0308-521x(00)00025-1

Hill, M. J., & Donald, G. E. (2003). Estimating spatio-temporal patterns of agricultural productivity in fragmented landscapes using AVHRR NDVI time series. *Remote Sensing of Environment, 84*(3), 367-384. doi: 10.1016/s0034-4257(02)00128-1

Hofstra, N., Haylock, M., New, M., Jones, P., & Frei, C. (2008). Comparison of six methods for the interpolation of daily, European climate data. *Journal of Geophysical Research-Atmospheres, 113*(D21), 19. doi: 10.1029/2008jd010100

Hundecha, Y., & Bárdossy, A. (2004). Modeling of the effect of land use changes on the runoff generation of a river basin through parameter regionalization of a watershed model. *Journal of Hydrology, 292*(1–4), 281-295. doi: http://dx.doi.org/10.1016/j.jhydrol.2004.01.002

Isidro, J., Alvaro, F., Royo, C., Villegas, D., Miralles, D. J., & del Moral, L. F. G. (2011). Changes in duration of developmental phases of durum wheat caused by breeding in Spain and Italy during the 20th century and its impact on yield. *Annals of Botany, 107*(8), 1355-1366. doi: 10.1093/aob/mcr063

Jacquemoud, S., Baret, F., Andrieu, B., Danson, F. M., & Jaggard, K. (1995). Extraction of vegetation biophysical parameters by inversion of the prospect plus sail models on sugar-beet canopy reflectance data - application to tm and aviris sensors. *Remote Sensing of Environment, 52*(3), 163-172. doi: 10.1016/0034-4257(95)00018-v

Jiang, Z. Y., Huete, A. R., Chen, J., Chen, Y. H., Li, J., Yan, G. J., & Zhang, X. Y. (2006). Analysis of NDVI and scaled difference vegetation index retrievals of vegetation fraction. *Remote Sensing of Environment, 101*(3), 366-378. doi: 10.1016/j.rse.2006.01.003

Jiapaer, G., Chen, X., & Bao, A. M. (2011). A comparison of methods for estimating fractional vegetation cover in arid regions. *Agricultural and Forest Meteorology, 151*(12), 1698-1710. doi: 10.1016/j.agrformet.2011.07.004

Jimenez-Munoz, J. C., Sobrino, J. A., Plaza, A., Guanter, L., Moreno, J., & Martinez, P. (2009). Comparison Between Fractional Vegetation Cover Retrievals from Vegetation Indices and Spectral Mixture Analysis: Case Study of PROBA/CHRIS Data Over an Agricultural Area. *Sensors, 9*(2), 768-793. doi: 10.3390/s90200768

Joyce, R. J., Janowiak, J. E., Arkin, P. A., & Xie, P. P. (2004). CMORPH: A method that produces global precipitation estimates from passive microwave and infrared data at high spatial and temporal resolution. *Journal of Hydrometeorology, 5*(3), 487-503. doi: 10.1175/1525-7541(2004)005<0487:camtpg>2.0.co;2

Karunaratne, A. S., Azam-Ali, S. N., & Steduto, P. (2011). Calibration and validation of fao-aquacrop model for irrigated and water deficient bambara groundnut. *Experimental Agriculture, 47*(3), 509-527. doi: 10.1017/s0014479711000111

Khan, M. R. (2011). *Crops from space : improved earth observation capacity to map crop areas and to quantify production.* (180), University of Twente Faculty of Geo-Information and Earth Observation (ITC), Enschede. Retrieved from http://www.itc.nl/library/papers_2011/phd/khan.pdf

Khoshravesh, M., Mostafazadeh-Fard, B., Heidarpour, M., & Kiani, A. R. (2013). AquaCrop model simulation under different irrigation water and nitrogen strategies. *Water Science and Technology, 67*(1), 232-238. doi: 10.2166/wst.2012.564

Lambert, J. J., Daroussin, J., Eimberck, M., Bas, C. L., Jamagne, M., King, D., & (eds)., L. M. (2003). Soil Geographical Database for Eurasia & The Mediterranean: Instructions Guide for Elaboration at scale 1:1,000,000, Version 4.0. (pp. 64). Luxembourg: Office for Official Publications of the European Communities.

Launay, M., & Guerif, M. (2005). Assimilating remote sensing data into a crop model to improve predictive performance for spatial applications. *Agriculture, Ecosystems & Environment, 111*(1–4), 321-339. doi: http://dx.doi.org/10.1016/j.agee.2005.06.005

Liu, Y. K., Mu, X. H., Qian, Y. G., Tang, L. L., Li, C. R., & Ieee. (2012). A vegetation phenology model for fractional vegetation cover retrieval using time series data *2012 Ieee International Geoscience and Remote Sensing Symposium* (pp. 3339-3342). New York: Ieee.

Lorite, I. J., Garcia-Vila, M., Santos, C., Ruiz-Ramos, M., & Fereres, E. (2013). AquaData and AquaGIS: Two computer utilities for temporal and spatial simulations of water-limited yield with AquaCrop. *Computers and Electronics in Agriculture, 96*, 227-237. doi: 10.1016/j.compag.2013.05.010

Ma, G., Huang, J., Wu, W., Fan, J., Zou, J., & Wu, S. (2013). Assimilation of MODIS-LAI into the WOFOST model for forecasting regional winter wheat yield. *Mathematical and Computer Modelling, 58*(3–4), 634-643. doi: http://dx.doi.org/10.1016/j.mcm.2011.10.038

Maas, S. J. (1988). Use of remotely-sensed information in agricultural crop growth-models. *Ecological Modelling, 41*(3-4), 247-268. doi: 10.1016/0304-3800(88)90031-2

Maisongrande, P., Duchemin, B., & Dedieu, G. (2004). VEGETATION/SPOT: an operational mission for the Earth monitoring; presentation of new standard products. *International Journal of Remote Sensing, 25*(1), 9-14. doi: 10.1080/0143116031000115265

Malet, P., Pécaut, F., & Bruchou, C. (1997). Beware of using cumulated variables in growth and development models. *Agricultural and Forest Meteorology, 88*(1–4), 137-143. doi: http://dx.doi.org/10.1016/S0168-1923(97)00042-7

McMaster, G. S., & Wilhelm, W. W. (1997). Growing degree-days: one equation, two interpretations. *Agricultural and Forest Meteorology, 87*(4), 291-300. doi: 10.1016/s0168-1923(97)00027-0

Mebane, V. J., Day, R. L., Hamlett, J. M., Watson, J. E., & Roth, G. W. (2013). Validating the FAO AquaCrop Model for Rainfed Maize in Pennsylvania. *Agronomy Journal, 105*(2), 419-427. doi: 10.2134/agronj2012.0337

Mkhabela, M. S., & Bullock, P. R. (2012). Performance of the FAO AquaCrop model for wheat grain yield and soil moisture simulation in Western Canada. *Agricultural Water Management, 110*(0), 16-24. doi: http://dx.doi.org/10.1016/j.agwat.2012.03.009

Moran, M. S., Alonso, L., Moreno, J. F., Mateo, M. P. C., de la Cruz, D. F., & Montoro, A. (2012). A RADARSAT-2 Quad-Polarized Time Series for Monitoring Crop and Soil Conditions in Barrax, Spain. *Ieee Transactions on Geoscience and Remote Sensing, 50*(4), 1057-1070. doi: 10.1109/tgrs.2011.2166080

Moriasi, D. N., Arnold, J. G., Van Liew, M. W., Bingner, R. L., Harmel, R. D., & Veith, T. L. (2007). Model evaluation guidelines for systematic quantification of accuracy in watershed simulations. *Transactions of the Asabe, 50*(3), 885-900.

Moriondo, M., Maselli, F., & Bindi, M. (2007). A simple model of regional wheat yield based on NDVI data. *European Journal of Agronomy, 26*(3), 266-274. doi: http://dx.doi.org/10.1016/j.eja.2006.10.007

Myneni, R. B., Maggion, S., Iaquinta, J., Privette, J. L., Gobron, N., Pinty, B., . . . Williams, D. L. (1995). Optical remote sensing of vegetation: Modeling, caveats, and algorithms. *Remote Sensing of Environment, 51*(1), 169-188. doi: http://dx.doi.org/10.1016/0034-4257(94)00073-V

Nash, J. E., & Sutcliffe, J. V. (1970). River flow forecasting through conceptual models part I — A discussion of principles. *Journal of Hydrology, 10*(3), 282-290. doi: http://dx.doi.org/10.1016/0022-1694(70)90255-6

Palosuo, T., Kersebaum, K. C., Angulo, C., Hlavinka, P., Moriondo, M., Olesen, J. E., . . . Rotter, R. (2011). Simulation of winter wheat yield and its variability in different climates of Europe: A comparison of eight crop growth models. *European Journal of Agronomy, 35*(3), 103-114. doi: 10.1016/j.eja.2011.05.001

Pandey, C. U. C. S. S. L. N. A. (2011). Synthesis of flow series of tributaries in Upper Betwa basin. *International journal of environmental sciences, 1*(7), 1459-1475.

Pettorelli, N. (2006). Using the satellite-derived NDVI to assess ecological responses to environmental change (vol 20, pg 503, 2005). *Trends in Ecology & Evolution, 21*(1), 11-11. doi: 10.1016/j.tree.2005.11.006

Piñeiro, G., Perelman, S., Guerschman, J. P., & Paruelo, J. M. (2008). How to evaluate models: Observed vs. predicted or predicted vs. observed? *Ecological Modelling, 216*(3–4), 316-322. doi: http://dx.doi.org/10.1016/j.ecolmodel.2008.05.006

Raes, D., Steduto, P., Hsiao, T. C., & Fereres, E. (2009). AquaCrop-The FAO Crop Model to Simulate Yield Response to Water: II. Main Algorithms and Software Description. *Agronomy Journal, 101*(3), 438-447. doi: 10.2134/agronj2008.0140s

Reed, B. C., Brown, J. F., Vanderzee, D., Loveland, T. R., Merchant, J. W., & Ohlen, D. O. (1994). Measuring phenological variability from satellite imagery. *Journal of Vegetation Science, 5*(5), 703-714. doi: 10.2307/3235884

Rötter, R. P., Palosuo, T., Kersebaum, K. C., Angulo, C., Bindi, M., Ewert, F., . . . Trnka, M. (2012). Simulation of spring barley yield in different climatic zones of Northern and Central Europe: A comparison of nine crop models. *Field Crops Research, 133*(0), 23-36. doi: http://dx.doi.org/10.1016/j.fcr.2012.03.016

Royo, C., Alvaro, F., Martos, V., Ramdani, A., Isidro, J., Villegas, D., & del Moral, L. F. G. (2007). Genetic changes in durum wheat yield components and associated traits in Italian and Spanish varieties during the 20th century. *Euphytica, 155*(1-2), 259-270. doi: 10.1007/s10681-006-9327-9

Royo, C., Aparicio, N., Blanco, R., & Villegas, D. (2004). Leaf and green area development of durum wheat genotypes grown under Mediterranean conditions. *European Journal of Agronomy, 20*(4), 419-430. doi: http://dx.doi.org/10.1016/S1161-0301(03)00058-3

Rubel, F., & Kottek, M. (2010). Observed and projected climate shifts 1901-2100 depicted by world maps of the Koppen-Geiger climate classification. *Meteorologische Zeitschrift, 19*(2), 135-141. doi: 10.1127/0941-2948/2010/0430

Salemi, H., Soom, M. A. M., Lee, T. S., Mousavi, S. F., Ganji, A., & KamilYusoff, M. (2011). Application of AquaCrop model in deficit irrigation management of Winter wheat in arid region. *African Journal of Agricultural Research, 6*(10), 2204-2215.

Santin-Janin, H., Garel, M., Chapuis, J. L., & Pontier, D. (2009). Assessing the performance of NDVI as a proxy for plant biomass using non-linear models: a case study on the Kerguelen archipelago. *Polar Biology, 32*(6), 861-871. doi: 10.1007/s00300-009-0586-5

Shapiro, S. S., & Wilk, M. B. (1965). An analysis of variance test for normality (complete samples). *Biometrika, 52*, 591-&. doi: 10.2307/2333709

Soddu, A., Deidda, R., Marrocu, M., Meloni, R., Paniconi, C., Ludwig, R., . . . Perra, E. (2013). Climate variability and durum wheat adaptation using the AquaCrop model in southern Sardinia. In N. Romano, G. Durso, G. Severino, G. B. Chirico & M. Palladino (Eds.), *Four Decades of Progress in Monitoring and Modeling of Processes in the Soil-Plant-Atmosphere System: Applications and Challenges* (Vol. 19, pp. 830-835). Amsterdam: Elsevier Science Bv.

Steduto, P. (2006). *Biomass Water-Productivity. Comparing the Growth-Engines of Crop Models*. Workshop Training Manual. Department of Agroenvironmental Sciences and Technology, University of Bologna.

Steduto, P., Raes, D., Hsiao, T., Fereres, E., Heng, L., Howell, T., . . . Geerts, S. (2009). Concepts and Applications of AquaCrop: The FAO Crop Water Productivity Model. In W. Cao, J. White & E. Wang (Eds.), *Crop Modeling and Decision Support* (pp. 175-191): Springer Berlin Heidelberg.

Stricevic, R., Cosic, M., Djurovic, N., Pejic, B., & Maksimovic, L. (2011). Assessment of the FAO AquaCrop model in the simulation of rainfed and supplementally irrigated maize, sugar beet and sunflower. *Agricultural Water Management, 98*(10), 1615-1621. doi: 10.1016/j.agwat.2011.05.011

Supit, I., & Wagner, W. (1999). Analysis of yield, sowing and flowering dates of barley of field survey results in Spain. *Agricultural Systems, 59*(2), 107-122. doi: http://dx.doi.org/10.1016/S0308-521X(98)00083-3

Tedeschi, L. O. (2006). Assessment of the adequacy of mathematical models. *Agricultural Systems, 89*(2–3), 225-247. doi: http://dx.doi.org/10.1016/j.agsy.2005.11.004

Todorovic, M., Albrizio, R., Zivotic, L., Saab, M. T. A., Stockle, C., & Steduto, P. (2009). Assessment of AquaCrop, CropSyst, and WOFOST Models in the Simulation of Sunflower Growth under Different Water Regimes. *Agronomy Journal, 101*(3), 509-521. doi: 10.2134/agronj2008.0166s

USDA, 2010. *Keys to soil taxonomy* (2010). Washington, D.C.: U.S. Dept. of Agriculture, Natural Resources Conservation Service : [Supt. of Docs., U.S. G.P.O., distributor].

USDA, 2012. USDA Office of the Chief Economist Crop Calendars http://www.usda.gov/oce/weather/CropCalendars/

Vandiepen, C. A., Wolf, J., Vankeulen, H., & Rappoldt, C. (1989). WOFOST - a simulation-model of crop production. *Soil Use and Management, 5*(1), 16-24.

Vanuytrecht, E., Raes, D., & Willems, P. (2014). Global sensitivity analysis of yield output from the water productivity model. *Environmental Modelling & Software, 51*(0), 323-332. doi: http://dx.doi.org/10.1016/j.envsoft.2013.10.017

Verhoef, W., & Bach, H. (2007). Coupled soil-leaf-canopy and atmosphere radiative transfier modeling to simulate hyperspectral multi-angular surface reflectance and TOA radiance data. *Remote Sensing of Environment, 109*(2), 166-182. doi: 10.1016/j.rse.2006.12.013

Vicente-Serrano, S. M., Saz-Sanchez, M. A., & Cuadrat, J. M. (2003). Comparative analysis of interpolation methods in the middle Ebro Valley (Spain): application to annual precipitation and temperature. *Climate Research, 24*(2), 161-180. doi: 10.3354/cr024161

Villegas, D., Aparicio, N., Blanco, R., & Royo, C. (2001). Biomass accumulation and main stem elongation of durum wheat grown under Mediterranean conditions. *Annals of Botany, 88*(4), 617-627. doi: 10.1006/anbo.2001.1512

Wellens, J., Raes, D., Traore, F., Denis, A., Djaby, B., & Tychon, B. (2013). Performance assessment of the FAO AquaCrop model for irrigated cabbage on farmer plots in a semi-arid environment. *Agricultural Water Management, 127*(0), 40-47. doi: http://dx.doi.org/10.1016/j.agwat.2013.05.012

Zeng, X. B., Dickinson, R. E., Walker, A., Shaikh, M., DeFries, R. S., & Qi, J. G. (2000). Derivation and evaluation of global 1-km fractional vegetation cover data for land modeling. *Journal of Applied Meteorology, 39*(6), 826-839. doi: 10.1175/1520-0450(2000)039<0826:daeogk>2.0.co;2

Zhao, H., Yang, Z. W., Di, L. P., & Pei, Z. Y. (2012). Evaluation of Temporal Resolution Effect in Remote Sensing Based Crop Phenology Detection Studies. In D. L. Li & Y. Y. Chen (Eds.), *Computer and Computing Technologies in Agriculture V, Pt Ii* (Vol. 369, pp. 135-150). Berlin: Springer-Verlag Berlin.